Cloud-based Real-time Continuous Bridge Monitoring: Bridge Weigh in Motion and Condition Assessment

A thesis submitted by

Zhiyong Zhao

In partial fulfillment of the requirements

for the degree of

Master of Science

in

Civil and Environmental Engineering

Tufts University

February 2017

Advisors: Masoud Sanayei, Ph.D.

Abstract

A cloud-based real-time bridge monitoring system was proposed in the research. Two possible applications of the real-time bridge monitoring system were studied. The first application used operational strain measurements to identify truck travel path, velocity, axle configuration, and total truck weight. The truck path is estimated by interpolating the relationship between the Girder Distribution Factors (GDFs) and truck path location. The truck velocity and axle configuration are estimated from the second derivative of strain measurements. The total truck weight is estimated using an influence line calibrated from a diagnostic load test performed with a known truck. The method is verified using strain data measured from daily truck traffic with known weights. The second application utilized detrended operational measured GDFs to detect possible bridge damages. A multiple regression model is fitted to the GDFs to study the factors that affect the GDFs. The multiple regression revealed that bridge age, temperature, frozen ground, and vehicle travel path are statistically significant explanatory variables for explaining most of the observed variability in GDFs. Using that regression model, the variations due to environmental factors and traffic events are removed from GDFs to eliminate those factors, leaving only the live load distribution due to the geometry of the bridge. A nonparametric rank-sum test is used to detect damage based on the resulting detrended GDFs. The bootstrap method is used to develop bridge signatures which assess the location of the damage. The proposed method is shown to exhibit a high degree of statistical power for detecting damages using operational detrended GDFs from strain measurements, resulting in both low probabilities of Type I and Type II errors.

Certificate of Fitness

Acknowledgments

I would like to thank my advisors Dr. Masoud Sanayei for his continued support and feedback on my research and personal development. Thanks to Dr. Rich Vogel and Dr. Alva Couch, for all their generous contributions to this research, for serving as my committee member, and for their kindly advices on developing my skills towards this.

Thanks to former Tufts graduate students: Jesse Sipple, John Phelps, Alex Reiff, and Chris Follen for building a solid foundation and providing resources for my research.

I am very grateful to work with doctoral candidate Nathen Davis, who provided me with substantial support and guidance. Nate was always willing to help, and always giving great suggestions. I would like to thank Jordan Weinsten for proofreading my manuscript and providing helps. I would like to thank my fellow graduate students: Hanshun Yu, Mingming Song, Ferris Masri, and Chao Zou. It has been a pleasure working with all of you.

I want to thank my parents for their continuously support in the past 26 years.

Finally, I would like to thank the love of my life Huiwen Chen, who has given me tremendous consistent support throughout my time at college and graduate school. I cannot make it without her.

Table of Content

List of Figures

Chapter 2

Chapter 3

Chapter 4

Appendix A

List of Tables

Chapter 1. Introduction

A large amount of bridges in the United States were built in the 1950s and 1960s. Many of these bridges have significantly deteriorated, exceeded their design life, carry heavier trucks, and experience higher Average Annual Daily Traffic (AADT). According to American Society of Civil Engineer (ASCE 2013), 25% of the bridge inventory in the United States are classified as structurally deficient or functional obsolete. Bridge safety has attracted considerable public attention in recent years. To ensure the safe operation of the existing bridges, information about daily heavy truck traffic (e.g., truck weights and number of axles) is needed to help evaluate bridge condition and to monitor overweight trucks for law enforcement. One of the purpose of this research is to develop an operation method to identify the truck configurations and truck total weight using strain measurements. Furthermore, the annual traffic volume and truck traffic with heavy cargos have increased significantly in past decades (FHWA, 2011). In order to maintain or improve current condition, the annual investment needed is $12.8 billion or $20.5 billion respectively (ASCE 2013). The high demand for future bridge management and maintenance requires improvements in efficiency to reduce costs. Another objective is to develop an operational method of real-time bridge health condition assessment.

The thesis is divided into four chapters. Two self-contained submitted journal articles are presented in Chapter 2 and 3. One conference paper is presented in Chapter 4. Chapter 2 presents a paper entitled “Bridge Weigh in Motion with Operational Strain Measurements”. The author develops a method that can identify truck travel path, velocity, axle configuration, and total truck weight using only strain measurements in Chapter 2. Operational truck traffic events are used to verify the proposed method showing that the method can extract truck information and estimate truck total weight. Chapter 3 manifests a paper entitled “Bridge Condition Assessment Using Detrended Operational Measured

Girder Distribution Factors". A multiple regression analysis of GDFs was performed finding that bridge age, temperature, frozen ground, and vehicle travel path are statistical significant to the GDFs for Powder Mill Bridge. Chapter 3 also discusses the findings that using hypothesis test and building bridge signature with detrended GDFs can assess the bridge structural health condition with high accuracy. In Chapter 4, a paper entitled "Cloud-based Real-time Continuous Bridge Monitoring for Condition Assessment" is introduced. References are listed at the end of each chapter. A cloud-based bridge structural health monitoring system is proposed for real-time continuous bridge condition assessment using measured detrended GDFs. A prototype of the proposed system using Microsoft Azure Virtual Machine and two lab computers is introduced in the Chapter. The Appendix A contains the additional figures for detrended GDFs method.

Chapter 2
Bridge Weigh in Motion with Operational Strain Measurements

2.1 Abstract

In this paper, a method for Bridge Weigh in Motion (BWIM) is developed to estimate unknown operational truck information using only a limited set of strain measurements. The information extracted from these strain gauge measurements includes truck path, velocity, axle configuration (number of axles and their spacing), and total truck weight. The truck path is estimated by relating the Girder Distribution Factors (GDFs) and truck path location. The truck velocity and axle configuration are estimated from the second derivative of strain measurements. The total truck weight is estimated using an influence line calibrated from a diagnostic load test performed with a known truck. The bridge influence line for the truck path is calibrated by solving a large sparse matrix from a linear system of equations. The calibrated strain influence line is proportional to the bending moment response at the midspan of center span when one axle weight is applied at a different location on the center span. Strains from the bottom of the girder nearest to the truck centerline are used to identify the axle configuration and velocity of the passing truck. This information is combined with the calibrated influence line to build the relationship between axle load and strain measurement. Using this relationship and the measured strain readings, the axle weight is calculated, and the total truck weight is determined. The method is verified using strain data measured from daily truck traffic with known weights.

2.2 Introduction

A large number of bridges in the United States were built in the 1950s and 1960s. Many of these bridges have significantly deteriorated, exceeded their design life, carry heavier trucks, and experience higher Average Annual Daily Traffic (AADT). As of 2015, more than 23% of the current bridge stock is structurally deficient or functionally obsolete

(USDOT, 2015). Bridge safety has attracted considerable public attention in recent years. To ensure the safe operation of the existing bridges, information about daily heavy truck traffic (e.g., truck weights and number of axles) is needed to help evaluate bridge condition and to monitor overweight trucks for law enforcement. Many technologies have been developed to monitor the weight of trucks, one of which is the Weigh-In-Motion system (WIM). WIM refers to the estimation of the weight of a moving vehicle and the portion of weight carried by each axle (ASTM International, 2009). There has been extensive research into WIM systems on highways and bridges in the US. Guo et al. (2004) compared three types of highway WIM systems consisting of using bending plates, load cells, and piezoelectric sensors embedded in or placed on the road surface.

There has been considerable progress in improving the WIM accuracy. In Europe, a large research project named Weigh in Motion of Axle and Vehicles for Europe (WAVE), was initiated in September of 1996 and lasted until June 1999. Many new technologies were proposed during the WAVE project that significantly enhanced WIM systems (WAVE, 2001). In the US, there are also some initiatives for improving WIM systems. The American Society of Testing and Material (ASTM) published standard specifications for WIM systems in the US in 2009 (ASTM International, 2009).

Even though these efforts have improved WIM systems, challenges remain when applying the current WIM system in some situations. Bending plate and load cells require embedment in the road, making installation and maintenance difficult. Piezoelectric sensors are placed on the road surface, which can disturb the traffic and can be inconvenient for maintenance. There is not a clear solution to solve these problems with the currently available WIM systems.

Bridge-Weigh-In-Motion (BWIM) is an alternative approach to WIM that is easy to install, maintain, and replace. Sensors such as strain gauges, accelerometers, and

tiltmeters may be installed on different bridge components at strategic locations and used to observe the bridge response to truck loading. The placement of sensors on various structural components makes the BWIM system an indirect method, where the principles of mechanics and structural analysis are used in truck identification. Compared with WIM, which is used to measure vehicle weight directly, BWIM is an inverse method that estimates the applied axle loads from the observed bridge response.

BWIM was initially introduced by Moses (1979), who compared the strain measurements beneath a bridge girder with the predicted analytical response from a structural model of the bridge. Least square error minimization was employed to determine the truck weights. In addition, Moses and Ghosn (1983) presented an algorithm to determine the weights of trucks from multiple lanes using an influence surface of strains. Since this work, many new methodologies have been developed in attempts to improve the accuracy of truck weight determination.

Many researchers have used field tests or results derived from finite element analysis to test proposed methods of identifying axle weights (Gonzalez and O'Brien, 1998, 2002; Ojio et al., 2000; Xiao et al., 2006; Zhao, 2010). Leming and Stalford (2002, 2003) used the truck–bridge interaction to develop a new BWIM algorithm. Gonzalez et al. (2012) proposed an algorithm using sensors at multiple longitudinal locations. Žnidarič et al. (2002), McNulty and O'Brien (2003), and O'Brien et al. (2006) obtained influence lines based on bridge measurements. O'Brien et al. (2008) reviewed the latest developments of BWIM and discussed promising methods for future development of BWIM, including moving force identification and Tikhonov regularization. Marques et al. (2016) proposed a BWIM method that adopts genetic algorithms to optimize the estimation of axle load of a train on a metallic railway bridge. Ojio et al. (2016) introduced a contactless BWIM

method with two cameras measuring bridge deflection. Yu et al. (2016) provided a comprehensive state-of-the-art review on BWIM technologies.

Quilligan et al. (2002) and Zhao et al. (2014) proposed two-dimensional (2D) algorithms for BWIM systems. The new, 2D version of the algorithm from Moses (1979) was used to identify axle weights from moving vehicles while considering the transverse distribution of the wheel loads on each girder. The algorithm was verified in field tests with the help of a commercially available SiWIM BWIM system, which includes weighing sensors and Free Axle Detectors (FAD).

Compared with conventional BWIM using FAD to identify vehicle axle configuration, axle detection without the use of sensors on the road surface is gaining increasing popularity. Wall et al. (2009) used the second derivative of measured strains to determine truck axle configuration and found the truck's weight by combining a load test-calibrated factor with the integrated strain response. Cardini and DeWolf (2009) used a long-term BWIM system for a simple span bridge. Using strain measurements and influence area method, they were able to identify truck weights without using axle detectors. O'Brien et al. (2012) studied the strategies for axle detection considering better positioning of strain sensors and a novel shear strain sensor. Yu et al. (2015) proposed a method that can identify vehicle axles utilizing wavelet analysis.

The objective of this research is to identify the travel path, speed, axle configuration, weight per axle, and the total weight of a passing truck using a true strain-response only method. Only 1 strain gauge per girder, at midspan on the bottom flange is required. The speed and axle configuration are identified using from the second derivative of the strain-response time histories, eliminating the need for FADs or cameras. The transverse position of the truck is identified using Girder Distribution Factors (GDFs) connecting the relative strain response at girder midspan to the truck centerline. The field-

calibrated influence line allows the determination of axle weights from the strain response of the girder nearest to the truck centerline. By combining the influence line methodology found in O'Brien (2006) with the methodology for identifying axle configuration found in Wall et al. (2009), the proposed methodology is capable of identifying unknown operational truck configurations and weight using only strain responses. No finite element model is required, and the method is highly computationally efficient.

Data from a truck diagnostic load test in 2011 is used to field-calibrate the influence lines and calculate the GDFs. Operational unknown truck information is then identified using strain measurements, and the results are verified against information measured directly from the trucks. This method proves capable of identifying truck travel path, speed, axle configuration, weight per axle, and total weight.

2.3 Powder Mill Bridge, Sensors, and Data Acquisition

The Powder Mill Bridge (PMB) is a steel-girder bridge located in Barre, Massachusetts. The PMB is 47 m long and has three continuous spans, as shown in Fig. 1. The center span has a length of 23.5 m and the end spans are 11.75 m long. There are six steel plate girders equally spaced at 2.25 m in composite action with a reinforced concrete deck. The bridge has two lanes, one northbound and one southbound. There is one sidewalk on the west side of the bridge. The Barre-Martone regional landfill and waste management center is located south of the bridge, less than a mile away. Heavy trucks destined for the landfill travel southbound over the bridge daily (Sanayei et al. 2012 & 2015). The onsite Data Acquisition (DAQ) system was installed during and after construction to collect continuous data from sensors installed on the bridge. Strain gauges were installed on the six steel girders at the steel fabrication facility prior to delivery. The bridge is a full-scale outdoor laboratory for setting up various short-term and long-term bridge response

measurements. Only six of the installed strain gauges are used for this research: one per girder, at midspan of the center span, installed on the bottom flange.

Fig. 1. Powder Mill Bridge (PMB) on Ware River in Barre, MA

When a vehicle crosses the bridge, the strain measurements are recorded by the DAQ system at a sampling frequency of 200 Hz. If the maximum strain reading exceeds a predefined threshold, the strain measurements are recorded and stored as a "truck event." The threshold for a truck event is defined to limit the amount of data to be analyzed by discarding data that does not produce strains consistent with a heavy truck crossing. Truck events that are measured while multiple vehicles are on the bridge simultaneously are also discarded (Reiff et al. 2016); the proposed method does not yet have the capability of weighing several vehicles simultaneously.

Each recorded truck event contains a time history of the strain measurements from the center span of the six girders. The strain measurements for a truck event are first filtered with a moving average filter (Vaseghi, 2008) to remove ambient vibrations and sensor/DAQ noise. In order to capture the live load strains due to the truck, each truck event was zeroed by subtracting the initial strain. Considering the period of time for each truck event was not long enough for a drastic temperature change, the strain gauge reading drift due to temperature change and environmental effects are not anticipated to be significant.

The strain measurements used in this research come from two time periods: (1) truck diagnostic load test performed in 2011, used to calculate the influence line and GDFs, and (2) operational truck events collected in 2016 to validate the proposed method.

2.4 Diagnostic Load Test on PMB

A diagnostic truck load test with known axle weights (Sanayei et al., 2012) was performed at the PMB in 2011, and strain response measurements (from the bottom flange at the center of the midspan) from the truck are shown in Fig. 2. The vehicle location during these tests was continuously monitored. Strain measurements taken from the load test in 2011 are used to calibrate an influence line correlating truck weight with girder midspan strains. The load test was performed with the same truck (**Error! Reference source not ound.**) for six different paths (Fig. 3) and each path was repeated three times. During the load test, the truck crossed the bridge at a constant crawl speed of about 1 m/s to limit any dynamic effects. The truck traveled northbound for all tests.

Fig. 2. The Truck Used in 2011 Truck Load Test

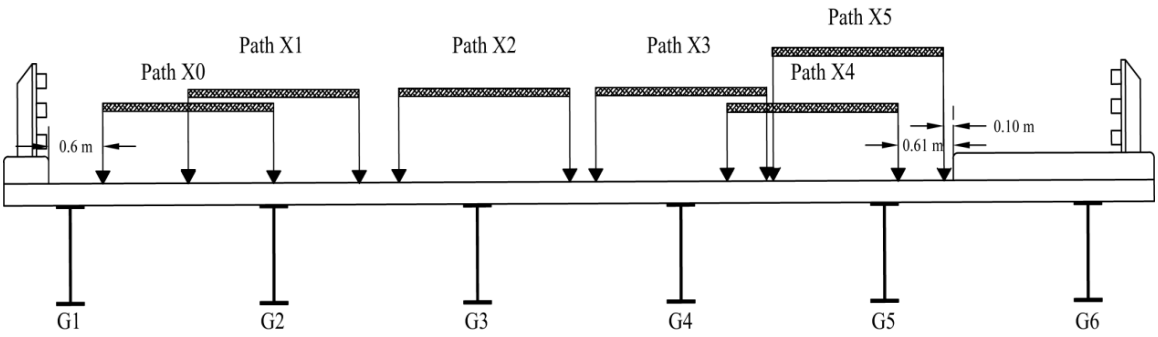

Fig. 3. PMB Truck Load Test Paths of 2011

Paths X1 and X3 roughly correspond to the southbound and northbound travel lanes, respectively. The 6 strain measurements recorded from the bottom flange at midspan of each girder during these two paths for a single run are plotted in Fig. 4.

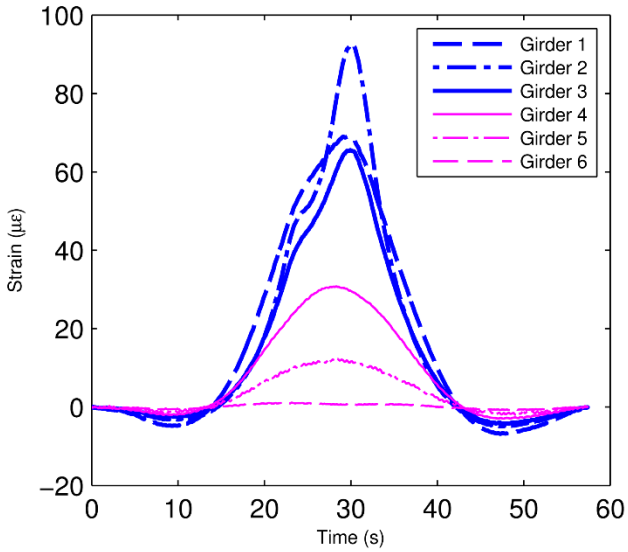

(a) Path X1 (Southbound Lane)

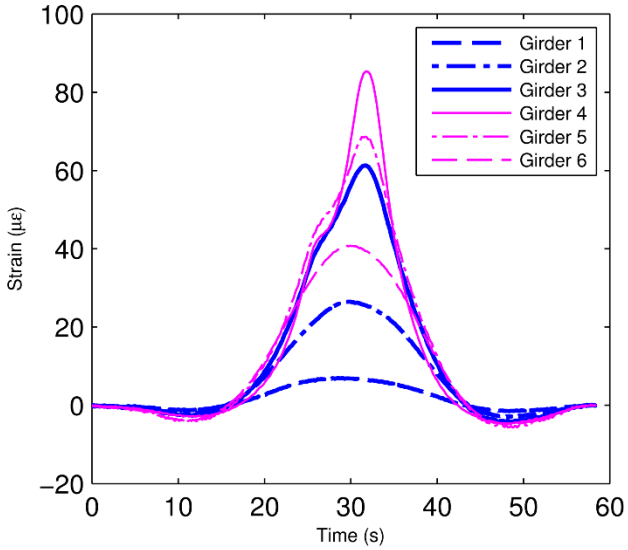

(b) Path X3 (Northbound Lane)

Fig. 4. Strain Measurements at the Center of Midspan of PMB for Truck Load Tests

The truck travel path is determined using Girder Distribution Factors (GDFs) which characterize the relative strains produced on the bottom flange of each girder during truck passage. Reiff et al. (2016) used a method for calculating the GDF from bottom flange strain measurements. For each girder, a polynomial fit of truck travel path versus GDF was developed using data from the 2011 load test. The truck travel paths were measured from the southbound lane curb to the truck centerline. A polynomial best-fit curve was found using GDFs calculated from bottom flange strain data from several tests with various known truck paths. A quartic polynomial was chosen as it as the best-fit curve, as higher order polynomial curves did not provide a significantly better fit.

The influence line relating midspan bending moment to a unit load is calculated from the 2011 load test. With a known truck weight and known truck speed, the measured strain response of the bridge can be used to calculate the bending moment influence line. While 6 separate influence lines exist for each truck path (1 per strain gauge), the strains from the girder nearest to the truck centerline path are used to calibrate the influence line, as that girder experiences the most significant strains and will have the best signal to noise

ratio. The calibrated influence line is used to identify truck axle weights during operational truck events.

2.5 Influence Line Methodology and Formulation

The diagnostic truck load test performed in 2011 is used to calculate the influence line between bending moment at midspan and a unit axle load. O'Brien et al. (2006) introduced a method for obtaining an influence line from the strain response of a bridge to a known truck. The method is based on least-square fitting to minimize the difference between analytical strains from the bending moment influence lines and measured strains. Moses (1979) proposed a scalar objective function based on the sum of the squared difference between analytical strains and measured strains, shown below in (1).

$$J = \sum_{j=1}^{M} (\varepsilon_j^a - \varepsilon_j^m)^2 \tag{1}$$

where J is the scalar objective function based on residual strains; ε_j^a is the analytical strain at data point j; ε_j^m is the measured strain at data point j; and M is the total number of measured data points with the truck on the bridge.

In order to obtain the analytical strains from a bending moment influence line, the relationship between strains and influence line is given by (2):

$$M_j = ES\varepsilon_j^a = \sum_{i=1}^{N} P_i I_{j-C_i} \tag{2}$$

where M_j is the bending moment of a girder at data point j; E and S are the Young's modulus and section modulus of the girder; P_i is the i^{th} axle load; I_{j-C_i} denotes the bending moment influence line for the corresponding axle load; and N is the total number of axles. C_i is the number of data points between i^{th} axle and the first axle, given by (3):

$$C_i = \frac{D_i f}{v} \tag{3}$$

where D_i is the distance between i^{th} axle and the first axle; V is velocity; and f is the sampling frequency.

For a given girder cross section, the Young's modulus and the section modulus are constant; meaning the bending moments are directly proportional to the strains. Meanwhile, the bending moments are equal to the sum of the bending moment generated by each axle load. The bending moment generated by each axle load is the product of the axle load, P, and the bending moment influence line, I. Therefore, the analytical strains can be expressed in terms of axle loads and influence line as:

$$\varepsilon_j^a = \frac{1}{ES}\sum_{i=1}^{N} P_i I_{j-C_i} \tag{4}$$

The influence line is calibrated using the 2011 test truck data. To calibrate the influence line, the derivative of the objective function with respect to all components of the influence line vector, $\{\mathbf{I}\}$ is set to be zero, as shown by (5).

$$\frac{\partial J}{\partial I_k} = 0 \tag{5}$$

where I_k is the k^{th} component of the influence line vector, $\{\mathbf{I}\}$, due to a single unit load. The strain measurement time history for a truck event begins with the truck's first axle entering the bridge, and ends with the truck's last axle leaving the bridge. As a result, the length of the influence line vector for a unit load is the number of data points from the test, M, minus the number of data points representing the length of the truck, C_N. The length of the influence line vector $\{\mathbf{I}\}$ is $M - C_N$.

The derivative of (4) is combined with (5) to obtain (6). The only non-zero terms from the summations in (6) are the terms where derivative of analytical strains with respect to I_k are not zero, which are limited to the terms where $k = j - C_i$.

$$\frac{\partial J}{\partial I_k} = \sum_{j=1}^{M} 2\left(\varepsilon_j^a - \varepsilon_j^m\right)\frac{\partial \varepsilon_j^a}{\partial I_k} = \sum_{j=1}^{M} \frac{2}{ES}\left(\varepsilon_j^a - \varepsilon_j^m\right)\sum_{i=1}^{N}\left(P_i \frac{\partial I_{j-C_i}}{\partial I_k}\right) = 0 \tag{6}$$

The j can be substituted with $k + C_i$ in (6) as:

$$\sum_{i=1}^{N} P_i \varepsilon^{m}_{k+C_i} = \sum_{i=1}^{N} P_i \varepsilon^{a}_{k+C_i} \tag{7}$$

The right part of (7) can be expended as:

$$\sum_{i=1}^{N} P_i \varepsilon^{a}_{k+C_i} = \frac{1}{ES} \sum_{i=1}^{N} P_i \sum_{n=1}^{N} P_n I_{k+C_i-C_n} \tag{8}$$

where P_n is the n^{th} axle load for separating index notation i.

For an example case where a three-axle truck crosses the bridge, (8) can be further expanded as:

$$\begin{aligned} ES\left(P_1\varepsilon^{m}_{k} + P_2\varepsilon^{m}_{k+C_2} + P_3\varepsilon^{m}_{k+C_3}\right) = {} & \left(P_1^{2} + P_2^{2} + P_3^{2}\right) I_k \\ & + \left(P_1P_2\right)\left(I_{k-C_2} + I_{k+C_2}\right) \\ & + \left(P_1P_3\right)\left(I_{k-C_3} + I_{k+C_3}\right) \\ & + \left(P_2P_3\right)\left(I_{k+C_2-C_3} + I_{k+C_3-C_2}\right) \end{aligned} \tag{9}$$

The measured load effect vector, $\{\boldsymbol{\varepsilon}\}$, of size $(M - C_3) \times 1$, is defined in (10) to represent the left side of (9).

$$\{\boldsymbol{\varepsilon}\} = ES \begin{Bmatrix} P_1\varepsilon^{m}_{1} + P_2\varepsilon^{m}_{1+C_2} + P_3\varepsilon^{m}_{1+C_3} \\ P_1\varepsilon^{m}_{2} + P_2\varepsilon^{m}_{2+C_2} + P_3\varepsilon^{m}_{2+C_3} \\ \cdots \\ P_1\varepsilon^{m}_{M-C_3} + P_2\varepsilon^{m}_{M-C_3+C_2} + P_3\varepsilon^{m}_{M} \end{Bmatrix} \tag{10}$$

The combination of (9) and (10) can be written in the matrix form as:

$$\{\boldsymbol{\varepsilon}\}_{(M-C_3)\times 1} = [\mathbf{W}]_{(M-C_3)\times(M-C_3)} \{\mathbf{I}\}_{(M-C_3)\times 1} \tag{11}$$

where $[\mathbf{W}]$ of size $(M - C_3) \times (M - C_3)$ represents a sparse symmetric matrix associated with the vehicle axle weights, defined by:

$$\begin{aligned} W_{i,i} &= P_1^{2} + P_2^{2} + P_3^{2} && i = 1 \cdots M - C_3 \\ W_{i,i+C_2} &= P_1P_2 && i + C_2 \le M - C_3 \\ W_{i,i+C_3} &= P_1P_3 && i + C_3 \le M - C_3 \\ W_{i,i+C_3-C_2} &= P_2P_3 && i + C_3 - C_2 \le M - C_3 \end{aligned} \tag{12}$$

The influence line vector $\{\mathbf{I}\}$ of size $(M - C_3) \times 1$ can be calculated when there is measured strain data for a known truck whose speed, axle spacing, and axle weights were measured. For the 2011 load test, the entire truck passage was recorded at the site, the truck axle spacing were measured with tape measures, and the truck axle weights were obtained

at nearby weigh station before and after the load test. Using the truck speed, truck axle spacing, and sampling frequency, the numbers of data points between the i^{th} axle and the first axle are calculated using (3). The sparse symmetric matrix $[\mathrm{w}]$ is constructed with the obtained information from the load test.

2.6 Influence Line Validation using Test Data

As stated earlier, six separate truck passage on six separate paths were performed in the 2011 truck load test. The influence lines for the six paths are obtained using (11). To demonstrate, the influence lines for Path X1 and Path X2 are shown in Fig. 5.

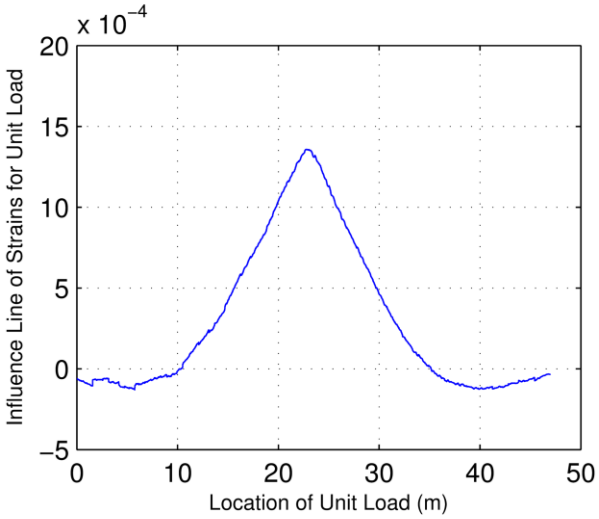

(a) Girder 1, Path X0

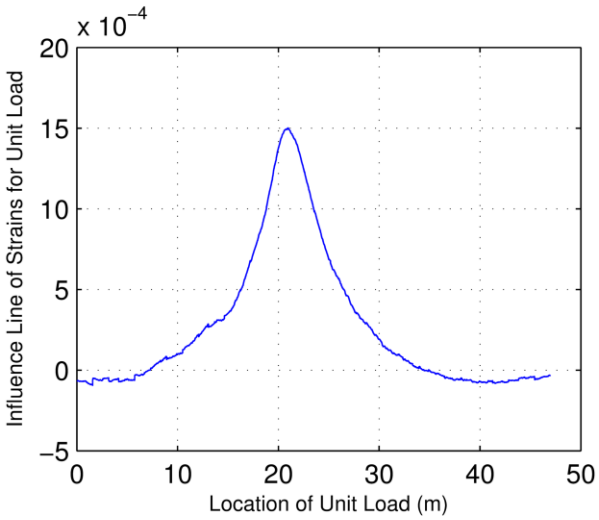

(b) Girder 2, Path X1

Fig. 5. Influence Lines of Strain

For each path, the influence line can be calculated for all six girders. In general, there are as many influence lines as the number of path multiplied by the number of girders. In this case, there are total 36 influence lines. Since averaging the identified influence line does not give better results and picking the influence line that is near truck travel path gives the most accurate results, only the single influence line that provides the best results is used for future total truck weight identification.

The influence line is verified by comparing the strains measured during the diagnostic load test with the predicted strain from the influence line shown in (4). E and S do not need to be known for this, as these terms cancel each other out and can be simply set to 1. The measured truck speed, axle spacing, axle weights, and the calibrated influence line are all required to calculate the predicted strains. The comparison between measured strain and predicted strain from the bending moment influence line are demonstrated in Fig. 6. Fig. 6a shows a case where neither of the truck wheels are directly above the girder, while Fig. 6b shows a case where the centerline of the truck is right above the girder. Both of these cases agree with the results of each other, indicating the calibrated influences lines

are valid. Now, for any future crossings by a truck whose axle configuration and speed are accurately known, the axle weights can be determined using these calibrated influence lines.

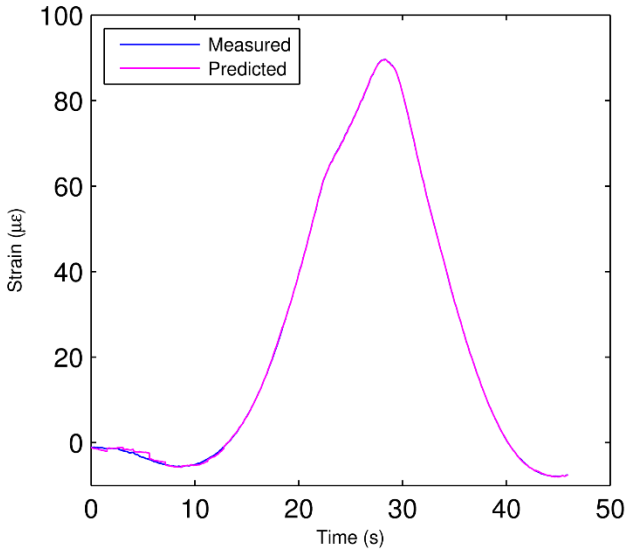

(a) Girder 1, Path X0

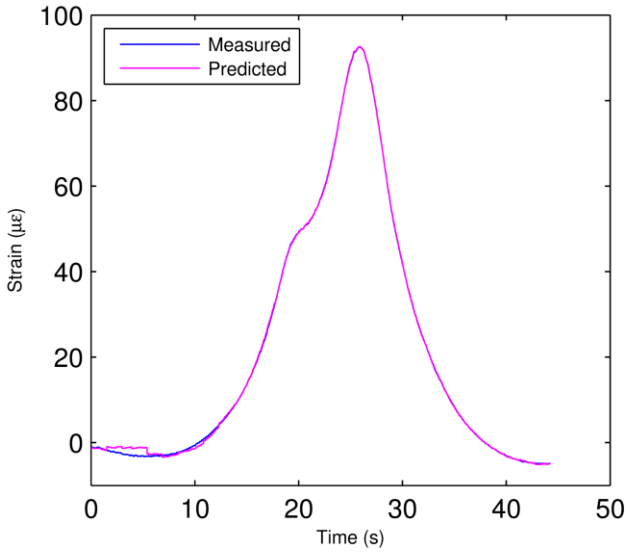

(b) Girder 2, Path X1

Fig. 6. Measured and Predicted Strain

2.7 Bridge Weigh-In-Motion Methodology

The sequence of identifying truck information from strain measurements is: identify an event with a single heavy truck, determine the travel path and speed of the truck,

find the number of axles, determine axle spacing, determine individual axle weights, and finally, calculate the total weight. The truck travel path is the transverse location of the truck on the bridge deck, assumed constant as the truck crosses the bridge. Once the truck travel path is determined, the strains from the nearest girders are used to identify the remaining truck information because the adjacent girders experience the greatest strain response. In order to identify the truck axle spacing, truck speed is required. Number of axles, axle spacing, and truck speed are required to find the axle weight with the influence line method.

2.7.1 Identify Truck Speed and Travel Path

The truck travel path is determined by using the fitted relationship between truck path location and the GDF. In Fig. 7, the red circles represent 5 load tests with different truck travel path (Since path X4 is very close to path X5, it was unnecessary to use path X5 in the GDF fitting.). The GDFs of girder 1 from the load tests are plotted against its corresponding travel path. A polynomial curve was fitted to the relationship between GDFs and truck travel path. This was performed for all girders. The transverse location of the centerline of an unknown truck is then found from this best fit curve. As an example, this interpolation is shown in Fig. 7 by using the GDF value to find the travel path. For each event, the truck travel path is determined by averaging the identified travel path from all girders.

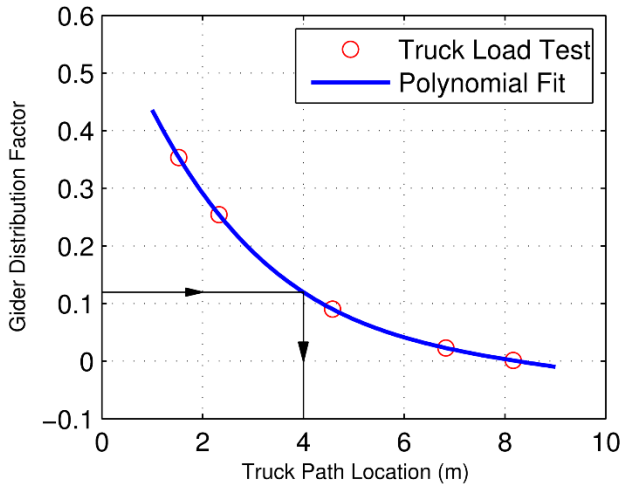

Fig. 7. Truck Travel Path and GDF Fit for Girder 1

To find the truck speed, there needs to be two reference points in the strain time history and a known distance from each other over which a passing truck can be clocked. Since the midspan strains are approximately zero as the centroid of a passing truck crosses each interior bent, it can be inferred from the time history when the truck crosses each pier. By knowing the distance between the two internal piers and the time taken to cross between them, the average truck speed over this distance can be found. However, since there is some rotational resistance at the piers, the strains at midspan go to zero when the centroid of truck is near, but not exactly over the piers. Due to this effect the distance between the two points on the strain time history is actually greater than the midspan distance. A time history of the bottom flange strain at midspan of Girder 2 from the 2011 test on path X1 is plotted in Fig. 8. The blue dashed line represents the instance in time when the truck centroid is near the pier locations and the midspan strains go to zero. For the 2011 truck load test, the average truck speed was calculated from the known length of the 3-span bridge, and the time that it took the truck to drive over the entire length (from saw cut to saw cut). $L_{midspan}$ was calculated by multiplying the average truck speed and the time it took from zero-to-zero strains for the midspan. It is assumed that the strain time histories of unknown future

trucks will have zero crossings at approximately the same locations as the test truck, so this calculated distance, $L_{midspan}$ is used to compute speed. It can also be seen in Fig. 8 that the midspan strain measurement changes sign as the truck centroid is between the two piers. This is consistent with the expectation of a positive bending moment in the middle of the center span while the truck centroid is between the two piers and a negative bending moment otherwise.

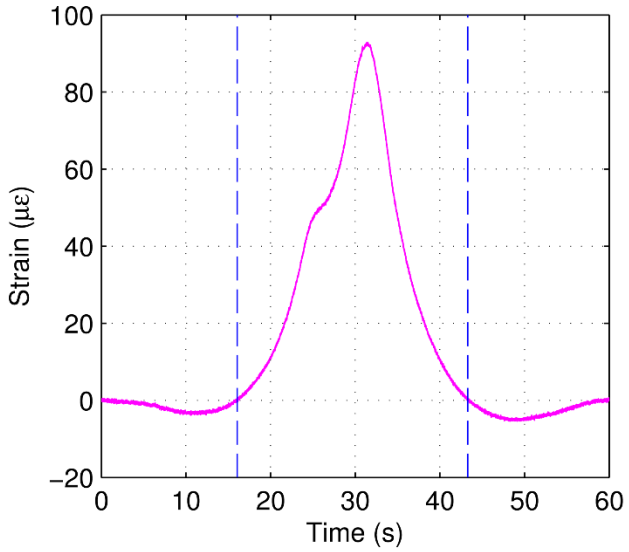

Fig. 8. Strain Measurements in 2011 Truck Load Test, Girder 2, Path X1

Assuming the velocity is constant as the truck passes the midspan strain gauge location, the average velocity for heavy trucks can be estimated by using (13).

$$v = \frac{L_{midspan}}{t_{midspan}} \tag{13}$$

Where $L_{midspan}$ is the distance between zero crossings in the strain time history in the 2011 truck load test, $t_{midspan}$ is the time it takes from zero-to-zero strain for mid span.

2.7.2 Identifying Truck Dimensions

In general, the second derivative of strain is proportional to the second derivative of the bending moment, as shown in (14) and (15). In order to illustrate this, two simple examples are given here. Fig. 9 shows the shear force and bending moment diagrams for a

simply supported beam subjected to a moving point load applied at the midspan. For this concentrated loading, the second derivative of moment is a Dirac delta function that shows an abrupt change in loading. The magnitude of the delta functions is the change in the shear force diagram, which is the magnitude of the point load. Therefore, each peak in the second derivative of measured strains indicates an axle loading at the location that the strains are recorded. Fig. 10 shows the shear and bending moment diagram of a three-span continuous beam with simple supports subjected to a three unit-load axle truck at three different time stops (a, b, and c). As the truck crosses the bridge, the girder shear at any stationary point only changes when an axle crosses that point, a three-axle truck will cause three shear changes at midspan as each axle crosses that point. This method can be used for trucks with higher number of axles for axle detection purposes.

$$M(t) = \frac{EI}{y} \cdot \varepsilon(t) \tag{14}$$

$$\frac{d^2\varepsilon}{dt^2} = \frac{y}{EI}\frac{d^2M}{dt^2} \tag{15}$$

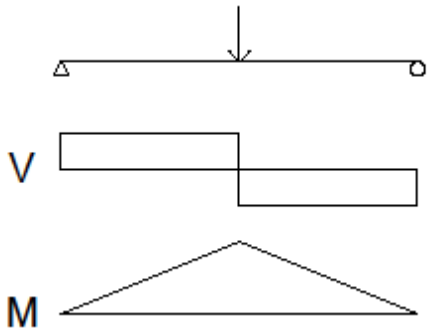

Fig. 9. Point Load on Simple Supported Beam

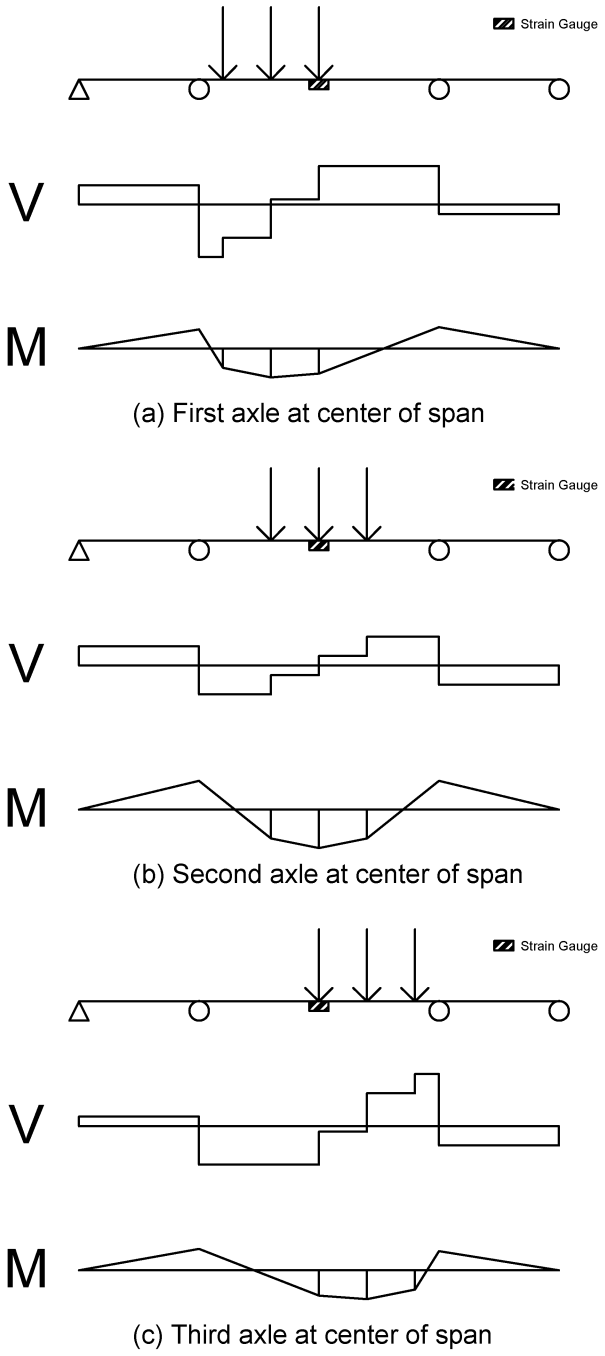

Fig. 10. Shear and Bending Moment Diagrams of a Three-axle Truck on Three-span Continuous Beam

Fig. 11 shows the ideal plot of second derivatives of strains for a moving truck with three axles providing unit loads. Each of the delta functions indicates a shear change at the midspan strain gauge location (i.e., truck wheel pass by). The three delta functions

represent configurations (a), (b) and (c), where an axle is located right above the midspan strain gauge. For other configurations, no axle is present over the midspan strain gauge location, there is no unit load, and the second derivative of the strain measurement is zero. Configuration (a) is the first detected delta function in the time history because the front axle is the first to arrive at the location of the strain gauge.

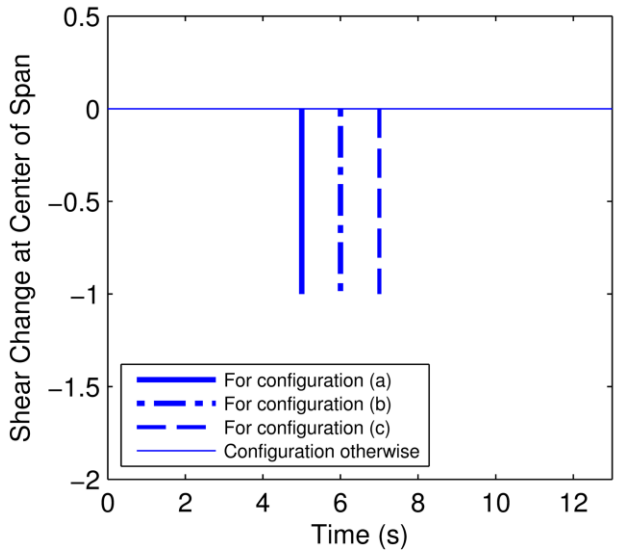

Fig. 11. The Time History of Shear Changes at Center of Span

In reality, the wheel loads from a passing truck are actually distributed loads on a small tire contact area and are not point loads. The implication of this fact is that the second derivative of measured strains does not include true delta functions and the peaks have some width. The strain measurements from the 2011 diagnostic truck load tests are used to verify this method of detecting axle locations. Before obtaining the strain second derivatives, the strain measurements are filtered with a moving average filter to reduce the impact of ambient vibrations and sensor noise. The data acquisition system used had low levels of electronic noise and the bridge dynamics due to the moving trucks on this stiff bridge were small. Fig. 12 shows the unfiltered measured strains and the filtered measured strains removing both low levels of vibrations and noise at midspan of Girder 1 from Path X1 in the 2011 load test. Since the noise of measured strains can be amplified for higher

derivatives, a differentiator filter is recommended by MATLAB to obtain the derivatives of data in order to reduce errors (MATLAB, 2016). A Finite Impulse Response (FIR) differentiator filter is designed to only include the frequency where the most of the signal energy is found but eliminate the noise frequencies. The goal of the differentiator algorithm is removing noise and errors caused by differentiating a signal as long as the peaks can be found. For 200 Hz sampling frequency, the filter order was 20 with a pass band frequency of 2 Hz and the stop band frequency of 3 Hz. The designed differentiator algorithm is used twice to obtain the second derivatives of the filtered strains as shown in Fig. 13. Each peak in the plot of strain second derivatives depicts the moment that an axle is right above the strain gauge. Using the time history of second derivatives of the measured strains, the time elapsed between axles passing the midspan strain gauge location is determined. By assuming the truck speed is constant during passage, the axle spacing is calculated.

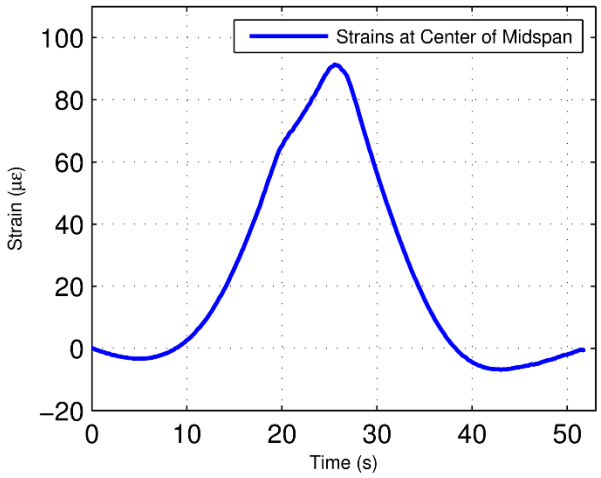

Fig. 12. Strains at Center of Midspan of Girder 1, Path X0

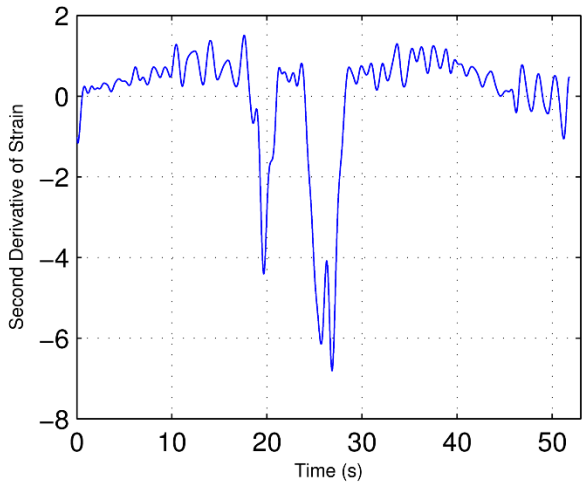

Fig. 13. Second Derivative of Strains of Girder 1, Path X0

2.8 Identify Total Truck Weight

The proposed method combines the methods that identify the number of axles, axle spacing, and truck speed with a method to find the axle weights and total truck weight from the influence line. Moses (1979) developed a method to find axle weights for a truck with a known axle configuration and speed. This method uses least square fitting to match the results to a calibrated influence line. The analytical strain can be calculated from the bending moment influence line and axle weight (16). The matrix $[IL]$ is an M by N matrix where M is the length of measured data points and N is number of axles. The matrix $[IL]$ is determined by using axle spacing and velocity. Each column of this matrix represents the bending moment response due to a unit axle weight. Each row of this matrix represents the moment response to a set of unit axle weights at one time.

$$\{\varepsilon^{a}\}_{M\times 1} = \frac{1}{ES}[IL]_{M\times N}\{P\}_{N\times 1} \tag{16}$$

The objective function in (1) can be written in matrix format as

$$
\begin{aligned}
J &= \left\{\left\{\varepsilon^a\right\} - \left\{\varepsilon^m\right\}\right\}^T \left\{\left\{\varepsilon^a\right\} - \left\{\varepsilon^m\right\}\right\} \\
&= \left\{\varepsilon^m\right\}^T \left\{\varepsilon^m\right\} - \frac{1}{ES}\left\{\varepsilon^m\right\}^T [IL]\{P\} \\
&\quad - \frac{1}{ES}\{P\}^T [IL]^T \left\{\varepsilon^m\right\} + \left(\frac{1}{ES}\right)^2 \{P\}^T [IL]^T [IL]\{P\}
\end{aligned} \tag{17}
$$

The derivative of error function with respect of axle load $\{P\}$ is set to be zero to minimize the difference between analytical strains and measured strains in (17).

$$
\frac{\partial J}{\partial \{P\}} = 0 - \frac{1}{ES}[IL]^T \left\{\varepsilon^m\right\} - \frac{1}{ES}[IL]^T \left\{\varepsilon^m\right\} + 2\left(\frac{1}{ES}\right)^2 [IL]^T [IL]\{P\} = 0 \tag{18}
$$

(18) can be simplified to obtain $\{P\}_{N\times 1}$ as

$$
\{P\} = ES\left[[IL]^T [IL]\right]^{-1} [IL]^T \left\{\varepsilon^m\right\} \tag{19}
$$

If ES is assumed to be 1 when calculating the influence line, the ES in (16) is also 1. Therefore, calculating ES is not necessary for this method to work. Based on the identified axle weights, the total truck weight can be calculated easily by summing up the axle weights.

2.9 Method Verification using Unknown Trucks

To provide verification of the proposed method, unknown truck events were collected on April 15, 2016. The bridge was marked with chalk so that truck travel paths could be determined from pictures taken during the passage. For verification of the proposed method, the total weight was measured and the axle configuration was recorded at the nearby Barre-Martone landfill immediately after the truck crossed the bridge.

The measured strains at midspan are recorded for all 6 girders at a 200 Hz sampling frequency. The travel path, speed, number of axles, axle spacing, and total weight of passing trucks were identified using the methods described in the previous sections. The identified truck information was compared with actual truck information to assess the performance of the method. In order to verify the proposed method, two aspects in

particular need to be verified: the accuracy of truck speed, number of axles, and axle spacing determination from the second derivative of strain measurements; and the accuracy of axle and total weight determination from the influence line. The speed and axle configuration of the truck are used to construct the matrix $[IL]$, which is then used to identify the axle weights. Several operational truck events were captured, however a few of them were disqualified for use with the BWIM because there was more than one vehicle on the bridge or truck was not traveling on the southbound lane. This method is focused on single vehicle event, for the future, other types of events shall be studied. **Error! Reference ource not found.** shows pictures of trucks A, B, and C taken at the PMB. In some cases, one truck axle was lifted up and not in contact with the bridge deck. A truck axle can be moved down in order to better distribute truck weights when passing over a bridge based on driver's judgment.

(a) Truck A (b) Truck B (c) Truck C

Fig. 14. Operational Trucks Identified

From the measured strains, the truck travel path is obtained to determine which girder's strain measurements and calibrated influence line shall be used. The truck speed is estimated using (13). The number of axles and axle spacing are identified from the strain second derivatives. Then the matrix $[IL]$ is constructed using the calculated influence line

and identified truck information. The influence line calibration was performed using the crawl speed load tests in 2011, which were all traveling in the northbound direction. The operational truck load identification was performed using the southbound traffic data since these trucks were headed to the landfill and thus, heavier. Since the axle weight influence lines are calculated for individual axle positions, the direction of travel does not affect the results, as long as the path is known. The matrix $[IL]$, formed from the field-calibrated influence lines and the measured truck configuration, is used to calculate axle weights as shown in (19). The total weight of the passing trucks is calculated and compared to the measurements taken at the landfill. Fig. 15 demonstrates that the predicted response using the influence line agrees well with the measured filtered response of operational truck A. This validates that the methodology used can accurately extract truck axle configurations and truck total weights from measured strain response of operational trucks.

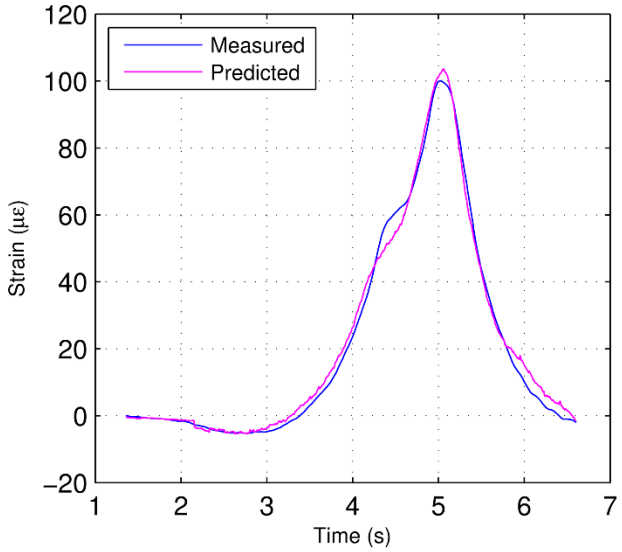

Fig. 15. Measured and Predicted Strain, Girder 2, Truck A

The identified results from the truck events are summarized in Table 1 to demonstrate the robustness of the proposed method. The travel path, number of axles, axle spacing, and total weight of three observed trucks is compared in Table 1. Truck speeds

are not compared because the test does not record the time that the truck uses to cross the bridge. By looking at the accuracy for identifying truck weights, which is the most important goal of this research, this method works well for all of the cases. Truck A has a highly accurate truck path, axle spacing and predicted truck weight. Truck B has a highly accurate truck path and truck weight but merged the rear axles to one. The total weight of Truck C was estimated the truck GVW with good accuracy, but there were errors identifying the number of axles and their spacing.

Table 1. Operational Trucks Identification

Truck	Speed (m/s)	Truck Path (meters)		Number of axles	Axle Spacings (meters)		Truck Weights (kips)	
		Measured/ Predicted	Error	Measured/ Predicted	Measured/ Predicted	Error	Measured/ Predicted	Error
A	8.02	3.15 / 3.16	0.5%	3/3	4.78 / 4.97, 1.30 / 1.44	4.0%, 10.8%	81.1 / 82.4	1.6%
B	8.95	3.13 / 3.14	0.2%	4/2	5.81 / 5.69	-2.1%	81.8 / 81.0	-1.0%
C	7.66	2.93 / 3.03	3.4%	3/2	5.81 / 5.56	-4.3%	80.2 / 83.0	3.5%

For truck A, the number of axles observed agrees with what is identified from strain measurements. For trucks B and C, however, the predicted number of axles doesn't agree with observations. The reason for the discrepancy between measured numbers of axles is that the peaks merge in the second derivative of strain when the rear axles are close to each other. Fig. 16 and Fig. 17, show the strain second derivatives for trucks A and B, respectively. The peaks associated with the rear axles of truck A are close, but separately identified. The peaks of associated with the rear axles of truck B merge to one peak in the strain second derivative plot. Truck C has the similar merged peaks as truck B. Merged peaks cause inaccurate prediction of axle spacing because the distance between peaks is not the distance between axles, but the distance between the front axle and the center of the rear axles. Measured axle spacing for trucks B and C are converted to the distance

between the front axle and center of the rear axles to compare with the predicted axle spacing. The incorrectly identified number of axles and axle spacing leads to inaccurately constructed matrix $[IL]$, which leads to an inaccurate estimation of axle weights in (19). It shall be noted that the truck BWIM information was determined based on calibrations using the 2011 truck load tests. As a result, if an operational truck path is away from the calibration path used, it might result in larger errors in truck weight estimations.

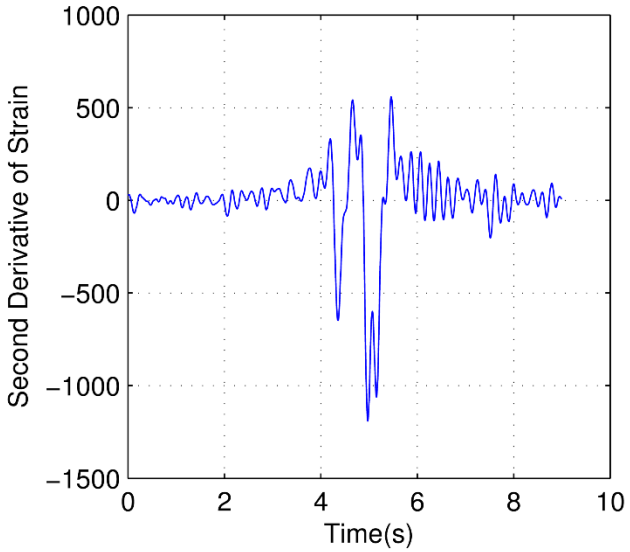

Fig. 16. Second Derivative of Strain for Truck A

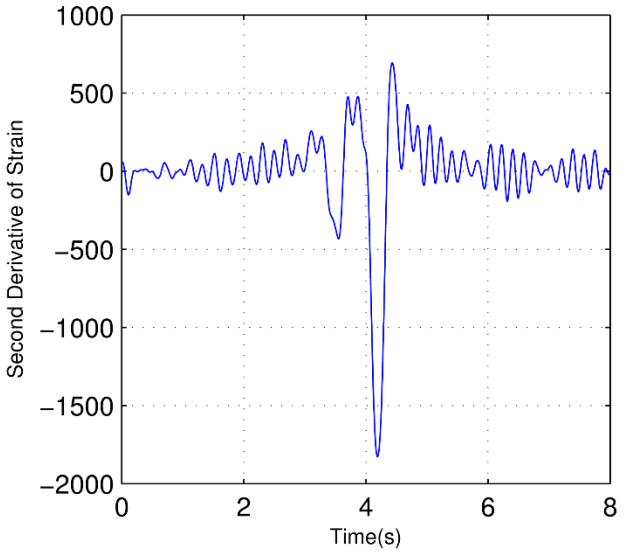

Fig. 17. Merged Peaks of Second Derivative of Strain for Truck B

2.10 Discussion

The factors that can make the peaks in the second derivatives of strains merge include small axle spacing, transverse positioning of the wheels with respect to the girders, truck speed, sampling frequency, signal noise level, and filtering techniques used.

The axle spacing and the distance between wheels and girders determines the gaps between the peaks in the second derivative of strains. When the girder is under or close to the truck wheels, the strain response experiences sharper changes because the shear change at the girder is also sharper. With larger axle spacing and less distance between wheels and girders, the gap between the peaks is wider and deeper. From Fig. 16, the gaps between the first and second peak is much larger than the gap between the second and third peak. Fig. 17 show only a single gap between the front axles and the rear axles, but with a much larger peak associated with the rear axles. Comparing trucks A and C, truck A's wheels are right above Girder 2, but none of the wheels of truck C are right above any girder. When a truck is traveling on the exact path and same direction that is used to calculate influence line, the identified axle weights, and truck gross weights is the most accurate. There were six total paths performed in the 2011 truck load test. The operational trucks that travel nearest to one of the six paths can be identified most accurately. Considering the space between the paths is not far, other trucks can also be identified with good accuracy.

The truck speed and sampling frequency determine the number of data points of strain measurements can be recorded for a truck event. With slower truck speed and higher sampling frequency, the amount of data points of an event is larger. Fig. 17 shows the second derivatives of strains for truck B, whose speed is larger than Truck A. For a given sampling frequency, the number of data points collected depends on the truck speed. With higher truck speed, less data points are collected resulting in merged peaks in the second derivatives of strains. Fig. 17 shows the increased speed of Truck B when compared with

Truck A may contribute to the merged peaks in the second derivatives of strains. Fig. 18 shows the second derivative of strain measurements of the same event for truck A, measured at 200 Hz and downsampled to 50 Hz for demonstration purposes. The 50Hz recording will lose frequency information over 25 Hz, leading to peak add-up when the two peaks are close to each other. For trucks traveling at highway speed, higher sampling frequency, possibly 1024 Hz is recommended to perform axle detection.

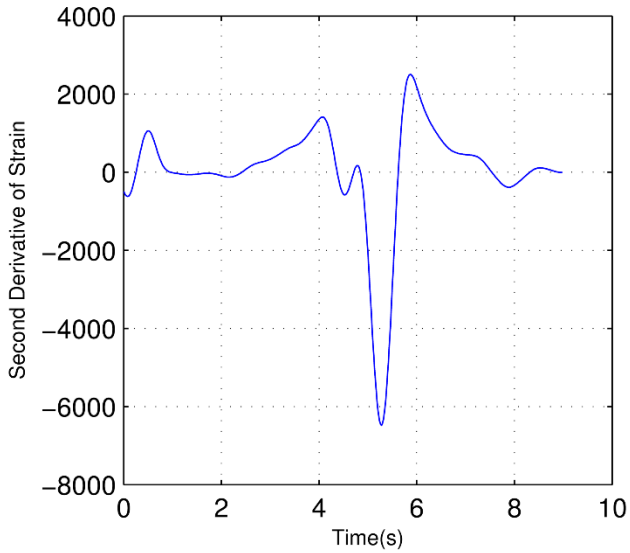

Fig. 18. Second Derivative of Strain for Truck A with 50Hz Sampling Rate

Noise level is also a factor that may make the peaks merge. With higher noise levels, a larger window of moving average filter is required, which also averages the gaps between the peaks especially when the gaps are small when the distance between the wheels and girders is larger than axles spacing. With modern DAQ systems and internal analog filters, the noise levels are low under normal conditions, if the system is configured and operated by a person who is knowledgeable with electronics, noise, filtering, and DAQ system capabilities.

2.11 Conclusions

In this research, a comprehensive Bridge Weigh-in-Motion method using strain measurements of a steel girder bridge was presented. The proposed methodology can

identify the configurations and weights of unknown operational trucks using only strain measurements. Truck travel path is identified by interpolating the GDFs with fitted polynomials curves. Truck speed is estimated from strain measurements by finding when the strain measurements change signs. Number of truck axles and their spacing are identified using the second derivative of strain measurement time histories, with the peaks designating the axle locations. The influence line of a unit load for a given path is calculated using a truck load test. Axle weights were calculated by minimizing the difference between measured and predicted strains from the influence line and the truck gross weight was determined from the summation of all axle weights. The new Bridge Weigh-in-Motion system is verified using operational strain measurements. For most of the cases, the method estimated the truck gross weight accurately. The identified truck information ranges from somewhat accurate to very accurate, however even the worst cases provide reasonable results. Thus, the new Bridge Weigh-in-Motion method is shown to be promising for monitoring oversize and overweight vehicles on bridges, helping to ensure Bridge structural health.

2.12 Future Works

Future work may focus on improving the method that identifies the truck information such as truck speed, number of axles, and axle spacing using bridge response measurements. The study of truck speed versus sampling frequency, signal noise, and filtering techniques can potentially improve the method. Future research about these factors can give better understanding about merging of the peaks in the second derivative of strain when the wheels are close to each other. By getting better results for identifying the number and spacing of truck axles, the method can improve the accuracy for truck weight estimation.

2.13 Acknowledgements

The authors are grateful for the funding of bridge instrumentation provided by the National Science Foundation (NSF) Partnerships for Innovation Grant No. 0650258, and funding for continued system upgrades provided by FHWA Long-Term Bridge Performance Program (Federal Contract No. DTFH61-08-00005, Subaward No. 00004397). Thanks to MassDOT and the town of Barre for access to the Powder Mill Bridge and Fay Spofford & Thorndike for sharing the design drawings and calculations. Additionally, the authors thank Geocomp Corp. for providing and assisting with the installation of the on-site data acquisition system and for continued technical support. Finally, the authors would like to thank Tony Qu who initiated this study.

2.14 References

ASTM International. “Standard Specification for Highway Weigh-In-Motion (WIM) Systems with User Requirements and Test Methods.” Designation: E 1318-09, West Conshohocken, PA, (2009): 1-16.

Cardini, A. J., and DeWolf, J. T. (2009). "Implementation of a long-term bridge weigh-in-motion system for a steel girder bridge in the interstate highway system." *J.Bridge Eng.*, 14(6), 418-423.

Gonzalez, A., & O’Brien, E.J. (1998). The development of a dynamic bridge weigh-in-motion algorithm. *Pre-proceedings of 2nd European conference on weigh-in-motion of road vehicles, Lisbon*, pp. 445–452.

Gonzalez, A., & O’Brien, E.J. (2002). Influence of dynamics on accuracy of a bridge weigh-in-motion system. *Proceedings of 3rd International Conference on Weigh-in-Motion (ICWIM3), Orlando, FL*. pp. 189–198.

Gonzalez, A., Dowling, J., O’Brien, E.J., & Z ˇ nidaricˇ, A. (2012). Testing of a bridge weigh-in-motion algorithm utilizing multiple longitudinal sensor locations. *Journal of Testing and Evaluation*, 40, 961–974.

Guo, L., Tang, Y., Yu, J., Li, J., Chen, X., and Liu, R. (2004). "Weigh-In-Motion System Design with Piezoelectric Sensor." Engineering Construction and Operations in Challenging Environments Earth and Space 2004: Proceedings of the Ninth Biennial ASCE Aerospace Division International Conference, 540-545.

Leming, S.K., & Stalford, H.L. (2002). Bridge weigh-in-motion system development using static truck/bridge models. *Proceedings of the American control conference, Alaska, USA*, pp. 3672–3677.

Leming, S.K., & Stalford, H.L. (2003). Bridge weighin-motion system development using superposition of dynamic truck/ static bridge interaction. *Proceedings of the American Control Conference, Denver, CO*, pp. 815–820.

Marques, F., et al. "Weigh-in-Motion Implementation in an Old Metallic Railway Bridge." *Engineering Structures* 123 (2016): 15-29.

MATLAB. "Take Derivatives of a Signal." Mathworks, http://www.mathworks.com/help/signal/ug/take-derivatives-of-a-signal.html Accessed 31 August 2016.

McNulty, P., & O'Brien, E.J. (2003). Testing of bridge weigh-in-motion system in a sub-Arctic climate. *Journal of Testing and Evaluation*, 31, 497–506.

Moses, F., and Ghosn, M. (1983). *Instrumentation for Weighing Trucks-in-Motion for Highway Bridge Loads*. No. FHWA-OH-83-001 Final Report. 1983.

Moses, F. Weigh-in-motion system using instrumented bridges. Transportation Engineering Journal of ASCE, Proceedings of the American Society of Civil Engineers, 1979, 105, No. TE3, 233–249.

O'Brien, E., Hajializadeh, D., Uddin, N., Robinson, D., and Opitz, R. (2012) "Strategies for axle detection in bridge weigh-in-motion systems" Proceedings of the 6th international WIM conference, Dallas, TX, 4-7 June, pp. 79-88. Hoboken, NJ: Wiley.

O'Brien, E., Znidaric, A., and Ojio, T. (2008). "Bridge weigh-in-motion-Latest developments and applications worldwide." *Proc., Int.Conf.on Heavy Vehicles*, 39-56.

O'Brien, E. J., Quilligan, M., Karoumi, R. (2006) "Calculating an influence line from direct measurements." Bridge Engineering, Proceedings of the Institution of Civil Engineers, 159 (BE1): 31-34

O'Brien, E. J., Znidaric, A., and Dempsey, A. T. (1999). "Comparison of two independently developed bridge weigh-in-motion systems." *Heavy Veh.Syst.*, 6(1), 147-161.

Ojio, T., Yamada, K., & Shinkai, H. (2000). BWIM systems using truss bridges. Proceedings of the 4th international conference on bridge management, Thomas Telford, University of Surrey, UK, pp. 378–385.

Ojio, T., Carey, C., O'Brien, E., Doherty, C., and Taylor, S. (2016). "Contactless Bridge Weigh-in-Motion." Journal of Bridge Engineering, 10.1061/(ASCE)BE.1943-5592.0000776, 04016032.

Quilligan, M., Karoumi, R., & O'Brien, E.J. (2002). Development and testing of a 2-dimensional multi-vehicle bridge-WIM algorithm. *Proceedings of the 3rd international conference on weigh-in-motion (ICWIM3)* (pp. 199–208).

Quilligan, M. J. (2003). "Bridge Weigh-in-Motion, Development of a 2-D Multi-Vehicle Algorithm." Licentiate Thesis.

Reiff, A. J., Sanayei, M., & Vogel, R. M. (2016). Statistical bridge damage detection using girder distribution factors. Engineering Structures, 109, 139-151.

Sanayei, M., Phelps, J. E., Sipple, J. D., Bell, E. S., and Brenner, B. R. (2012). "Instrumentation, nondestructive testing, and finite-element model updating for bridge evaluation using strain measurements." *J. Bridge Eng.*, 17(1), 130-138.

Sanayei, M., Alexandra J. Reiff, Brian R. Brenner, and Gregory R. Imbaro, (2015) "Load Rating of a Fully Instrumented Bridge: Comparison of LRFR Approaches," Journal

of Performance of Constructed Facilities, Online in March 2015, Paper in April 2016, Paper No. 04015019. doi:10.1061/(ASCE)CF.1943-5509.0000752

U.S. Department of Transportation (2015). Highway statistics. Retrieved from http://www.fhwa.dot.gov/bridge/structyr.cfm

Vaseghi, S. V. (2008). Advanced digital signal processing and noise reduction. John Wiley & Sons.

Wall, C. J., Christenson, R. E., McDonnell, A. H., and Jamalipour, A. J. (2009). "A Non-Intrusive Bridge Weigh-in-Motion System for a Single Span Steel Girder Bridge Using Only Strain Measurements ." Rep. No. CT-2251-3-09-5, Federal Highway Administration.

WAVE. "Weigh-in-motion of Axles and Vehicles for Europe." General Report, LCPC, (2001).

Xiao, Z.G., Yamada, K., Inoue, J., & Yamaguchi, K. (2006). Measurement of truck axle weight by instrumenting longitudinal ribs of orthotropic bridge. *ASCE Journal of Bridge Engineering*, 11, 526–532.

Yu, Y., Cai, C.S., and Deng, L. (2016). "State-of-the-art review on bridge weigh-in-motion technology". Advances in Structural Engineering, doi:10.1177/1369433216655922.

Yu, Y., Cai, C.S., and Deng, L. (2015). "Vehicle axle identification using wavelet analysis of bridge global responses". Journal of Vibration and Control, doi:10.1177/1077546315623147.

Zhao, H. (2010). Bridge weigh-in-motion for bridge safety and maintenance (Doctoral dissertation). Department of Civil, Construction, and Environmental Engineering, University of Alabama at Birmingham, Alabama, USA.

Zhao, H., Uddin, N., Shao, X., Zhu, P., and Tan, C. (2015) "Field-calibrated influence lines for improved axle weight identification with a bridge weigh-in-motion system." *Structure and Infrastructure Engineering*, 11:6, 721-743, DOI: 10.1080/15732479.2014.904383

Zhao, H., Uddin, N., O'Brien, E. J., Shao, X., and Zhu, P. (2014). "Identification of vehicular axle weights with a bridge weigh-in-motion system considering transverse distribution of wheel loads." *J.Bridge Eng.*, 19(3).

Z ˇnidaricˇ, A., Lavricˇ, I., & Kalin, J. (2002). The next generation of bridge weigh-in-motion systems. In B. Jacob & E.J. O'Brien (Eds.*), Proceedings of 3rd international conference on weigh-in-motion (ICWIM3)* (pp. 219–229).

Chapter 3
Bridge Condition Assessment Using Detrended Operational Measured Girder Distribution Factors

3.1 Abstract

Long-term operational strain measurements are used from a three-span continuous bridge with steel girders to estimate Girder Distribution Factors (GDF) which are used to detect bridge damages. A multiple regression model is fitted to the GDFs to study the factors that affect the GDFs. The multiple regression revealed that bridge age, temperature, frozen ground, and vehicle travel path are statistically significant explanatory variables for explaining most of the observed variability in GDFs. Using that regression model, the variations due to environmental factors and traffic events are removed from GDFs to eliminate those factors, leaving only the live load distribution due to the geometry of the bridge. A nonparametric rank-sum test is used to detect damage based on the resulting detrended GDFs. The bootstrap method is used to develop bridge signatures which assess the location of the damage. The proposed method is shown to exhibit a high degree of statistical power for detecting damages using operational detrended GDFs from strain measurements, resulting in both low probabilities of Type I and Type II errors. In damage scenario simulations, the proposed method could detect damage when it exists with a high level of confidence, and it did not issue false alerts when the damage was not present. The proposed operational, non-parametric, and non-FEM-based method using only measured strains is highly computing-efficient and can be used for real-time monitoring of bridges for condition assessment.

3.2 Introduction

According to USDOT (2015), 38% of bridges in the United States were built 50 years ago, 10% are structurally deficient, and 14% are functionally obsolete. Furthermore, the annual traffic volume and truck traffic with heavy cargos have increased significantly

in past decades (FHWA, 2011). The high demand for future bridge management and maintenance requires improvements in efficiency to reduce costs. Currently bridges should be inspected every 24 months, according to National Bridge Inspections Standards Regulation (Federal Highway Administration, 2004). However, visual bridge inspections can often be subjective and inconsistent (Moore et. al 2001). A bridge structural health monitoring and condition assessment system can provide an objective assessment to supplement a visual bridge inspection. Such a system monitors the strain response of the bridge to traffic events, assesses the bridge health by comparing the response with the range of values expected of a healthy bridge, and sends early alerts for bridge management and maintenance planning.

Many different methods are used to detect bridge damages. These methods can be classified by the type of data used, by its source of excitation, and by the index used. Some methods use both structural excitation data (input) and response data (output), and others only use only response data. The excitation can be static, dynamic, or ambient. The measurements can be accelerations, strains, tilts, displacement, or other forms of physical response measurements. This research utilizes output-only measurements, operational traffic excitations, and strain measurements for structural damage detection. The purpose of choosing such an approach is the ease of application in practice and the reduction of costs. The proposed method does not require finite element models, thus it is computing efficient to apply it to many different bridges. There will be no bridge closure in this method, which is favorable for bridge owners and drivers. Strain gages are less expensive compared to other measurement devices with the same level of accuracy.

The bridge live load distribution factor is the ratio of live loads carried by each girder and the overall live loads when a vehicle crosses the bridge. The American Association of State Highway and Transportation Officials (AASHTO) provides equations

for calculating the distribution factors to determine the percentage of designed load carried by each girder (2010). The AASHTO distribution factors are appropriately conservative compared to the distribution factors that are calculated from strain measurements. A Girder Distribution Factor (GDF) is defined as the percentage of total live load carried by a bridge girder when the girders are identical (Ghosn et al. 1986). The sum of GDFs for each girder equals to one, which means all the live loads are carried by the girders. When the girders have different stiffness, which is true for the Powder Mill Bridge (PMB), the GDFs do not represent the true distribution of live loads, but rather can be used to compare the peak strains of girders relative to one another. If these alternative GDFs change for the same vehicle that crosses the bridge on the same path in the same condition, the change in GDFs indicates the change in girder load sharing, which is often indicative of bridge damage. The GDF is defined by

$$GDF = \frac{\varepsilon_i}{\sum_{j=1}^{N} \varepsilon_j} \tag{20}$$

Where ε_i denotes the strain measurements from the ith girder.

Damaged bridges experience a change of stiffness that is reflected in the way in which loads are distributed over the structure (Kim et. a., 2008; Comanducci et. al., 2016). The GDF is an effective indicator of bridge damage that has been used in several studies. Enright and Frangopol (1999) used the change in GDFs after girder damage to find the critical damage case in their bridge reliability analysis. Wipf et al. (2006) monitored the changes in GDFs to evaluate the health and performance of a bridge over time. Cardini and DeWolf (2009) constructed an envelope of acceptable GDFs with measured strains. They found that a damaged girder would produce a GDF below envelope values. Plude (2011) utilized GDFs to examine the observability of different damage cases, creating an envelope of acceptable values of GDFs. Reiff et al. (2016) developed a statistical framework to detect

bridge damages based on the results of repeated hypothesis tests evaluating changes in the probability distribution of observed GDFs. Whelan and Gangone (2015) summarized their findings of GDFs as a means for structural diagnostics and performed an analysis of the effect of measurement uncertainties on GDFs.

GDFs can be affected by many factors. Nowak and Hong (1991) showed that GDFs change with different girder spacing and span length. Bishara et al. (1993) found that bridge skew angle influences GDFs for simply supported composite I-beam bridges. Eom and Nowak (2001) investigated GDFs for steel girder bridges, specifying the influence on GDFs by span length, girder spacing, composite action, and support conditions. Tabsh and Tabatabai (2001) showed that the transverse location of a truck would affect GDFs. Eamon and Nowak (2002) studied the effect on GDFs of adding edge-stiffening elements (barriers and sidewalks) and diaphragms. To summarize, there are at least three types of factors reported in literature that can alter GDFs: 1) bridge geometry and conditions, 2) vehicle transverse location, and 3) support stiffness conditions. The first type of factors can be assumed constant in a short time period but may be affected by deterioration. The second and third types of factors can vary from differing traffic events and environmental effects. These non-structural effects would introduce errors when utilizing GDFs as an indicator of bridge structural damages.

In this study, multiple linear regression is employed to develop a multivariate model of GDFs that depends on numerous exogenous non-structural factors, which enables us to remove those non-structural effects. Even though linear regression is used to fit the multivariate model, the model is nonlinear because some of its elements are nonlinear, such as the travel paths. The method used in this research is referred to as multiple regression. The concept and method of multiple regression can be found in a typical regression textbook such as that by Draper and Smith (2014). The objective is to develop a model that

explains as much of the variability in the GDF measurements as possible, which when accomplished can be used to remove environmental and traffic effects on the GDFs so that the remaining model noise only contains information relating to potential bridge damage. Linear regression is a powerful tool to fit a statistical model of a dependent variable that can be used for removing unwanted effects from extraneous parameters. Since there is more than one factor that affects the GDFs, the regression model shall include all independent factors to fully capture the behavior of GDFs. In structural engineering field, multiple linear regression has been used in research by Guan and Vistas (2008), Jin et al. (2015), Kromanis and Kripakaran (2014).

Follen et al. (2014) introduced a bridge signature as the "expected response of a bridge structural system to daily traffic as measured by an instrumentation system". They collected peak strains from heavy truck events to develop a suite of nonparametric cumulative probability distributions, which represent the probabilistic behavior of a healthy bridge. Bridge signature envelopes can be developed from nonparametric prediction intervals using the bootstrap method. Reiff et al. (2016) extended the ideas by Follen et al. (2014) with a statistical decision and hypothesis testing framework. The research discussed in this article extends the idea of statistical hypothesis testing and bridge signatures introduced by Reiff et al. (2016) and Follen et al. (2014), respectively. This research introduces a method for removing the variation of non-structural factors to increase the overall accuracy of bridge structural damage detection and localization. This detrending method is applied to measured GDFs prior to damage assessment. The proposed operational, non-parametric, and non-FEM-based method using only measured strains is highly computing-efficient and can be used for real-time monitoring of bridges for condition assessment.

In this research, long-term measured strain and temperature data are used to calibrate the multiple regression models of GDFs. The variation of GDFs due to non-structural and environmental effects is removed based on the resulting models, resulting in detrended GDFs which exhibit only potential damage. In the proposed system, the detrended GDFs, instead of GDFs, are used to improve the accuracy of bridge damage detection. The nonparametric rank-sum test is adopted to identify the damage (Wilcoxon, 1945). The bridge signature is utilized to locate and quantify the bridge damages. The authors also examine the likelihood of Type I errors, defined as issuing a bridge damage alert for a healthy bridge, and the likelihood of Type II errors, defined as not issuing an alert when the bridge is damaged. The proposed method is shown to achieve low levels of both Type I and Type II errors.

3.3 Data Acquisition and Data Processing

The PMB is a three-span steel girder bridge in Barre, Massachusetts, as shown in Fig. 19. There are six composite steel plate girders that are in composite action with a reinforced concrete deck. The six girders are equally spaced at 2.25 m on centers. The PMB carries traffic in both directions with two lanes. A 1.8-meter-wide sidewalk is located on the east side of the bridge. The cross section of the PMB is shown in Fig. 20. The PMB as a full-scale laboratory has over 200 sensors installed during and after the construction. There are 100 strain gages that were installed on the six steel girders before the girders were placed. Only six of the strain gages located at the midspan of the center span will be used in this research.

Fig. 19: Picture of PMB and DAQ System

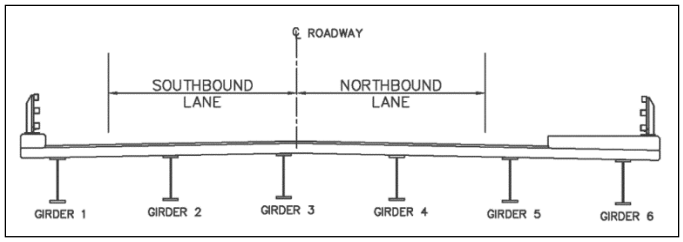

Fig. 20: Cross Section of PMB

When a vehicle crosses the bridge, the strain responses are recorded by the Data acquisition (DAQ) system with a 50 Hz sampling frequency. A traffic event is defined and collected as a segment of the strain measurements if the maximum strain reading exceeds a predefined threshold. The record length of traffic events depends on vehicle speeds and vehicle length. The threshold is defined to limit the amount of data to be collected to analyze the bridge's health condition by discarding small vehicles that produce small strain response of the bridge. For a busy bridge, the higher threshold can reduce the amount of data to be analyzed but give the intended information for bridge structural health monitoring. The strain threshold used in this research is 40 micro strain, following the research by Follen et al. (2014), which only keeps the response data of excitement from heavier vehicles and trucks. The temperature of the steel girders is also recorded during each traffic event.

Traffic events that involve multiple vehicles simultaneously are automatically identified and discarded. The proposed method does not have the capability to use the strain response of the bridge when there are multiple vehicles on the bridge simultaneously. To

remove traffic events with multiple vehicles, single vehicle events shall be identified. A single vehicle event is the traffic event in which there is only one vehicle on the bridge. Typical southbound and northbound events are shown in Fig. 21 and Fig. 22. For a southbound event, the strain measurements of girders near southbound lane are larger. The distribution of strain measurements for the northbound traffic events are similar. Events with vehicles traveling in the same direction and in the opposite directions are shown in Fig. 23 and Fig. 24, respectively. For events with vehicles travelling in the same direction, the peaks in strain measurements are not closely spaced, and the maximum strain reading comes from different girders. For events with vehicles travelling in opposing directions, the larger strain measurements switch from girders 1, 2, and 3 to girders 3, 4, and 5. A routine was programmed to run at the bridge to automatically discard the multiple-vehicle events and the small single-vehicle events. It saves only the larger single-vehicle events and performs statistical modeling, regression analysis, and hypothesis testing.

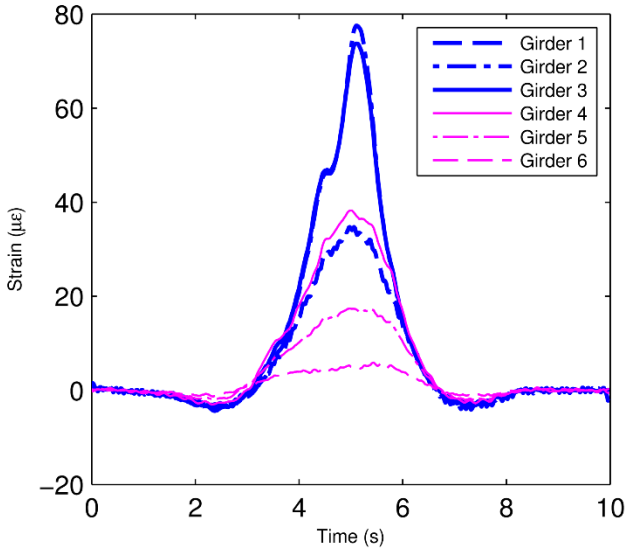

Fig. 21: Typical Southbound Single Vehicle Event

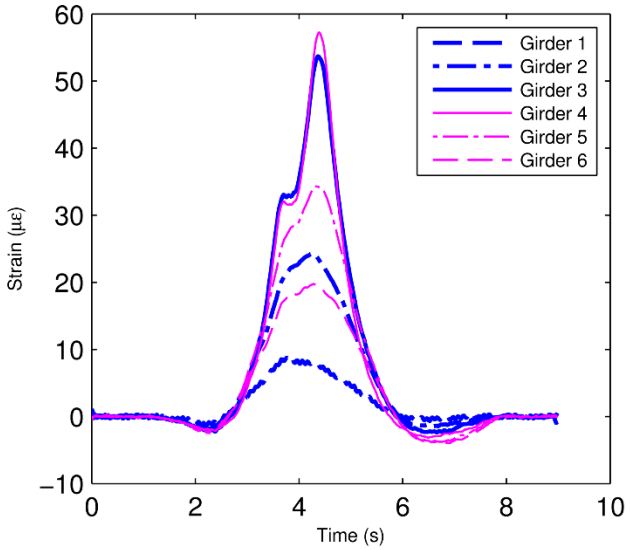

Fig. 22: Typical Northbound Single Vehicle Event

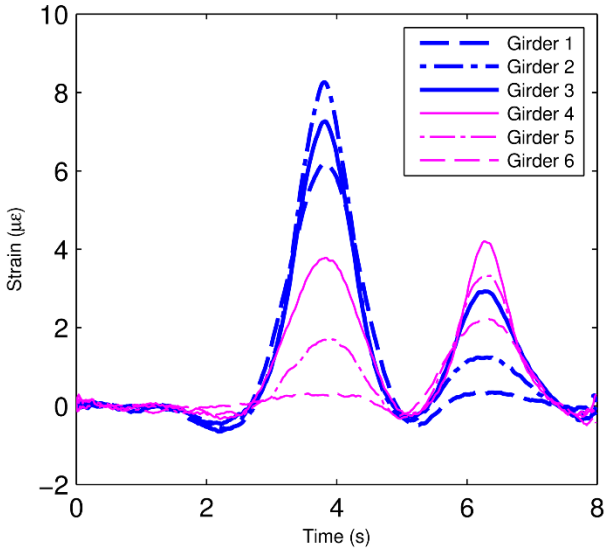

Fig. 23: Two Vehicles Traveling in the Opposite Direction

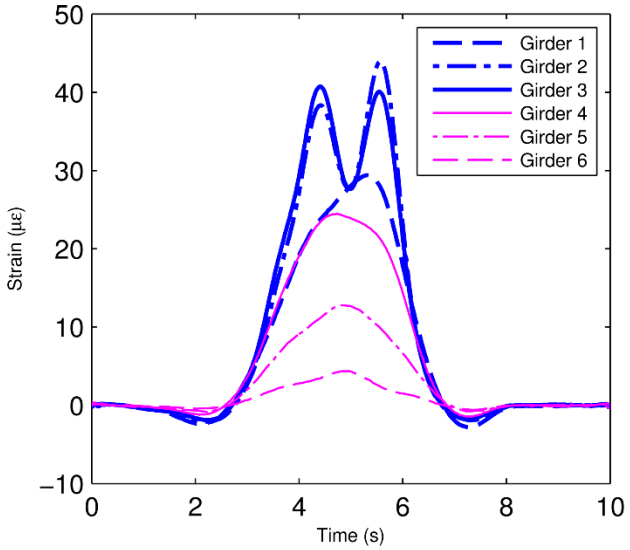

Fig. 24: Two Vehicles Traveling in the Same Direction

3.4 Multiple Regression Models for Girder Distribution Factor

3.4.1 Background

GDFs provide an index of bridge health, however they are affected by operational and environmental factors, including but not limited to bridge age, temperature, frozen ground, and vehicle travel path. Structural and non-structural factors both can affect GDFs. The structural factors, such as bridge geometry, concrete deck thickness, girder dimensions, support stiffness, etc., can be assumed to be constant unless the bridge is damaged. The non-structural factors will vary for different traffic event loadings and for different environmental conditions. The probabilistic properties of GDFs are studied to evaluate whether bridge structural damage can be detected. A quantile plot can be used to describe the steady state cumulative probability distributions (cdf) of the GDFs. Such a cdf will exhibit variability about its steady state value if an inadequate number of observations are used in its construction or if the GDFs were collected from different seasons and environmental conditions. Here a nonparametric empirical quantile function is employed to express the cdf of the GDFs by plotting the ordered values of the GDF versus their exceedance probabilities computed using the Weibull plotting position $p_i = i/(n+1)$ where

i is the rank of the observation. The Weibull plotting position yields unbiased estimates of the exceedance probabilities regardless of the underlying distributions of the GDF observations. For example, the 0.2 quantile corresponds to the value of a GDF which is greater than 20% of all values. In Fig. 25, the GDF of girder 2 for 0.8, 0.6, 0.4, and 0.2 quantiles are plotted for all acceptable traffic events collected for 12 months. The events are added in chronological order. Fig. 25 illustrates that the GDF distribution is not stable due to seasonal effects and that it varies widely for this girder. If the GDF distribution were stable, it would eventually reach a steady state value for large sample sizes. The other five girders exhibited the same behavior as illustrated in Fig. 25, indicating that there are operational and environmental factors affecting the measured strain data.

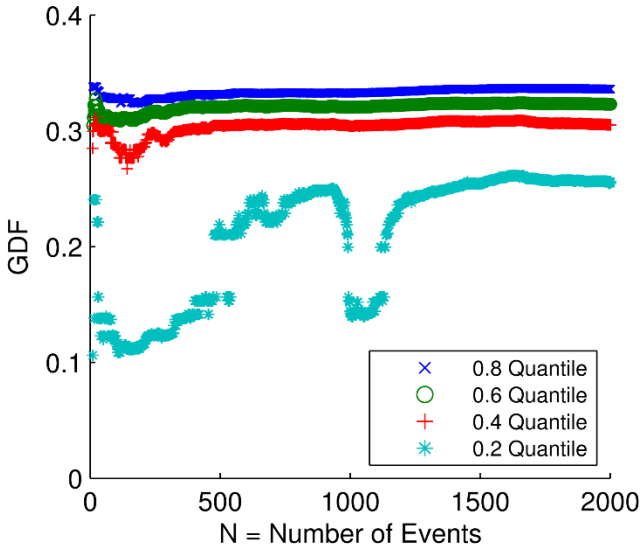

Fig. 25: Quantile Plot of GDF for Girder 2

3.4.2 Formulation of the Regression Model

The variability observed in values of GDFs can result in inaccuracies in the resulting damage alerts. The cdf of the GDFs collected during winter are different than the cdf of the GDFs collected during summer. The cdf of the GDFs from southbound events differ from the cdf of the GDFs corresponding to northbound events. The bridge damage detection system that is based on hypothesis testing results can result in false positive alerts

if the GDFs distributions are dependent on seasonal effects and vehicle travel paths. To ensure accurate detection of changes in the distribution of the GDFs, those external factors that affect the behaviors of GDFs can be removed to provide a consistent index for bridge damage detection, as is shown below.

For modeling the GDF value for a particular girder, it is hypothesized that bridge age, temperature, frozen ground, and vehicle travel path are related to the behavior of the GDF and can thus be used to construct the multiple regression model in (21) with the following variable definitions: X_D is the number of years since completion of construction, X_T is the girder temperature during the traffic event, X_F is either zero or one to account for the effect of frozen ground and snowbank conditions, and X_P is the vehicle travel path.

$$GDF = \beta_0 + \beta_1 X_D + \beta_2 X_T + \beta_3 X_F + \beta_4 X_P + \beta_5 X_P^2 + \beta_6 X_P^3 + Residual \quad (21)$$

Our goal is to first estimate the regression model in (2) and then to use the resulting model to remove the variation due to the non-structural effects, leading to detrended GDF values that can only be influenced by potential damage. The detrended GDF will preserve the structural-related information that will be used for damage assessment. New traffic events will also be detrended using this regression model to compare with the calibrated healthy range of detrended GDFs.

3.4.3 Justification of the Regression Model

As discussed in the introduction, there are at least three types of factors reported in literature that can affect GDFs: 1) bridge geometry and conditions, 2) vehicle transverse location, and 3) support stiffness condition. To represent the three types of factors, bridge age, temperature, frozen ground, and vehicle travel path are used in the multiple regression.

The bridge geometry is assumed to be constant during the data collection period because this bridge is recently constructed and the authors frequently visually checked that there was no damage to the bridge. The stiffness of bridge components determines how the

live loads are distributed, which affects the GDFs. It is not necessarily true that the relationship between the stiffness of a certain bridge component and its GDF is linear. However, the changes in stiffness for a healthy bridge due to environmental effects or short-term deterioration are in a relatively small range compared to the changes for a damaged bridge or long-term deterioration. In this initial research, the GDFs are assumed to change linearly with the change in the stiffness from environmental effects and short-term deterioration. The assumptions for simplified linear relationships can be verified by evaluating the goodness-of-fit for the regression model. If the regression model can mimic the behavior of GDFs with these assumptions, it is not necessary to use higher order relationships.

Deterioration effects may change the thickness of the concrete slab and thus the moment of inertia of the girder in the long term. The bridge deterioration can be modeled as bridge components deteriorated at different rate (Mašović& Hajdin, 2014), where the stiffnesses of different bridge components change at different rates. However, it is also well established that bridge deterioration is positively correlated with bridge age (Busa et al., 1985; Chen and Johnston, 1987; Madanat and Ibrahim, 1995; Madanat et al., 1995; Frangopol et al., 1997; Goyal et al., 2016). Because the PMB was recently constructed, there is not enough information about deterioration process of the bridge. Bridge age is calculated as the number of days since construction of the bridge was completed, and it can be used to estimate the deterioration process. The relationships between the GDFs and bridge age are simplified to be linear because the traffic events used were collected during 1 year.

The temperature variation influences the stiffness of ground soil, concrete deck, steel girders, and elastomeric bridge bearing pads. The authors performed literature reviews of the relationship between temperature and the stiffnesses of these bridge components.

Laloui and Cekervac (2003) studied the influence of temperature variation above freezing point on the elastic modulus of soil. Christ et al. (2009) found the relationship between soil elastic modulus and temperature below freezing point. Dahmani et al. (2007) showed the relationship between the elastic modulus of concrete and temperature. Fukuha and Sanpei (1993) and Ledbetter (1981) studied the elastic modulus of steel with temperature variation. Stanton and Roeder (1982) and Stanton et al. (1999) indicated that low temperature could cause a significant increase in the stiffness of elastomeric bridge bearings. Alampalli (2000) found that the accumulated moisture at supports might freeze to cause partial fixity, resulting in an increase of stiffness. In the preliminary regression model, the effects of temperature on all components of the bridge are lumped into a single linear model between temperature and the GDFs. For more detailed detrending it is possible to model separate parameters of the bridge that might be temperature dependent (for example, ground soil stiffness, bridge bearing pads stiffness, ice buildup in expansion joints, snow bank locations, and elastic moduli of concrete and steel). However, the preliminary study is performed to assess whether a more detailed study with more temperature related parameters is required.

Since the relationship between temperature and ground soil stiffness is different for frozen and unfrozen ground soil, as is the existence of a snowbank developed along the roadside during winter, a binary variable is used to quantify the different conditions and is set to either zero or one. The frozen ground process varies based on the type of soil: ice forms more easily in loose soils than in dense soils (NSIDC, 2016). The development of the snowbank also varies with precipitation. To simplify the model, the transition between different conditions is neglected.

A bridge girder will carry more load if the truck path is close to it. The vehicle travel path is defined as the distance from the vehicle centerline to the face of southbound lane curb. The relation between vehicle travel path and GDFs of all girders are shown in

Fig. 26. Polynomial relationships between vehicle travel path and all GDFs appeared to yield a reasonable approximation of the behavior of GDFs. The authors used polynomials of various orders approximate the shape of data in Fig. 8, and the 3rd order polynomial was the lowest-order model that led to uniformly good results for all girders. Given bridge geometry and environmental conditions, the relationships between GDFs and vehicle travel path are fitted to 3rd order polynomials.

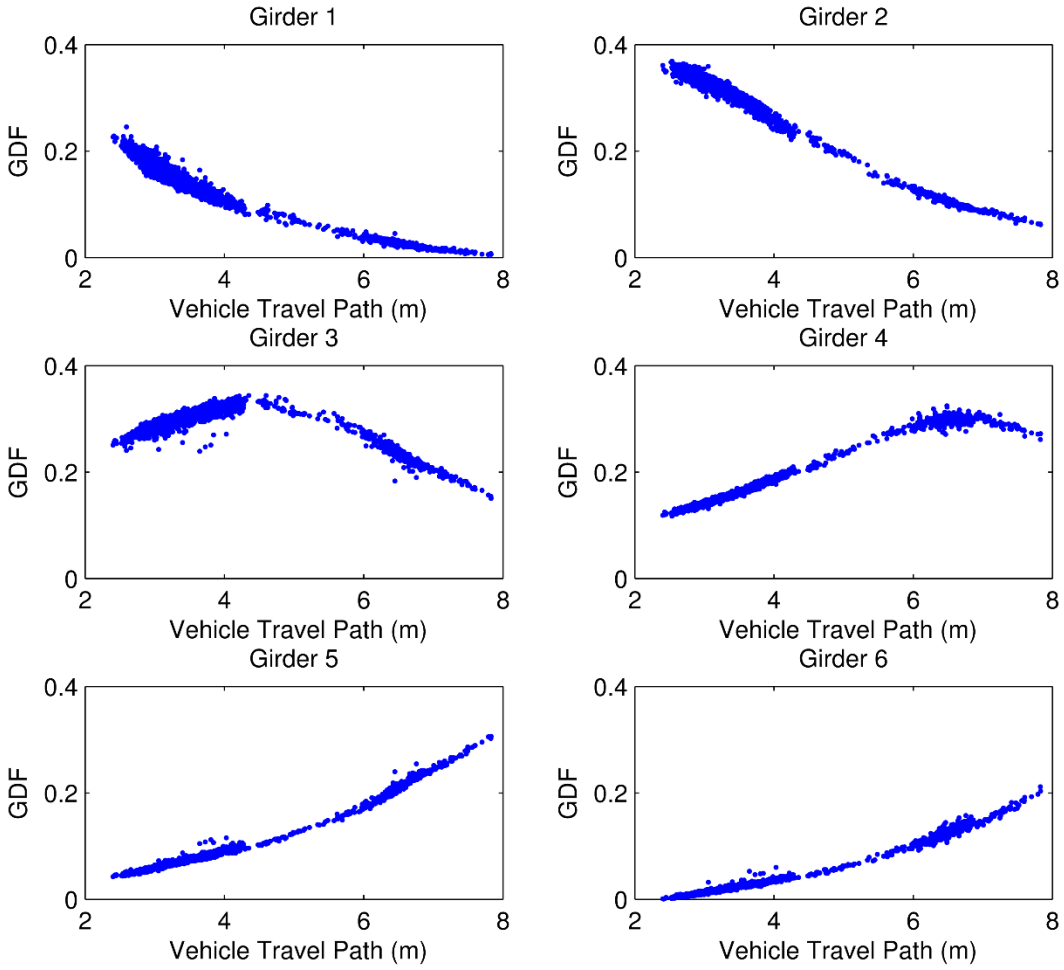

Fig. 26: Relationships between Vehicle Travel Path and GDFs of All Girders

The regression model residuals, or errors, are defined as the differences between the model estimates of GDFs and the corresponding observed values. In a perfect model,

the residuals would all be zero. In reality, residuals contain at least three types of errors: modeling errors, model parameter estimation errors, and measurement errors. Modeling errors exist because important explanatory variables may be left out and because the true model form is unknown. Only the explanatory variables that are suspected to significantly affect the response are included in our preliminary model. Measurement errors arise from sensor calibration and electronic noise as well as digitization and filtering. Model parameter errors arise from the limited sample sizes with which the model in (2) can be estimated.

3.4.4 Multivariate Model Development

The Ordinary Least Squares (OLS) method is used to calculate the regression coefficients in (1), which also enables the estimation of standard errors and T-values associated with the regression coefficients. An important benefit of multiple regression is the ability to perform statistical hypothesis tests on the significance of each regression model coefficient. Such tests all depend critically on assumptions concerning the behavior of the regression model residuals. The four critical assumptions are that the residuals have a mean of zero, are approximately normally distributed, are independent of time, and exhibit constant variance (homoscedasticity). Under these conditions, p-values corresponding to estimated model coefficients can be obtained from a Student's t-test associated with each regression model coefficient. Here the GDFs are the responses, or dependent variables, and the bridge age, temperature, frozen ground, and travel path are the four predictors, or explanatory variables. The regression analysis generates an equation to describe the relationship between predictor variables and the response variable and can be subjected to rigorous hypothesis testing, as is shown below.

Regression coefficients represent the mean change in the response variable corresponding to one unit of change in the predictor variable while holding other predictors

in the model constant. The standard errors of the regression coefficients measure the statistical accuracy of the estimated coefficients. The t-value is a test statistic that measures the difference between an observed sample statistic and its hypothesized population parameter in terms of the standard error. The t-value of each model coefficient is calculated by dividing the coefficient by its standard error. The t-test can be used to determine the statistical significance of each regression coefficient which is termed its p-value, computed as the exceedance probability associated Students-t distribution corresponding to the estimated t-value for each model coefficient.

The p-value of each term tests the null hypothesis that the corresponding model coefficient is equal to zero, which would mean that the factor has no influence on the GDFs. Here the typical limit for a p-value is assumed as 0.05. A low p-value, which is less than 0.05, indicates that one can reject the null hypothesis because the possibility that the coefficient equals zero is less than 5%. In other words, a model coefficient that has a low p-value implies that its associated predictor variable is likely to be a meaningful contributor to the model because changes in the predictor's value are said to be significantly related to changes in a particular response variable. Conversely, a large p-value, which is greater than 0.05, suggests that changes in the predictor are possibly not significantly associated with changes in the responses. The p-values are typically used to determine which predictors shall be kept in the regression model, and they are useful for this task as long as the model residuals behave as described above.

Once the predictors are shown to be statistically significant for predicting the GDFs, the regression model must be verified to ensure that it can capture most of the variation of GDF observations. A common goodness of fit metric, R-squared, is the percentage of the response variation that is explained by a model. R-squared represents the ratio between the variation from the model and the total variation in the original GDF data.

An adjusted R^2 is employed in the evaluation of regression model. This metric is preferred in a multivariate setting because it accounts for artificial inflation in R^2 resulting from the addition of more than one explanatory variable in the regression.

3.4.5 GDF Regression Model Using PMB Data

To fit the regression relationships between the GDFs and the predictor variables, a total of 2259 measured traffic events during a continuous 12 months and the associated temperature data are used. The GDFs for each independent traffic event are calculated from the measured strains at the midspan of the center span. Bridge age is obtained by counting the dates of each traffic event. Vehicle travel path is estimated by interpolating the calculated GDFs with the fitted relationships between GDFs and travel path from a 2011 truck load test. The method for estimating vehicle travel path was verified with measured operational events where the difference between the estimated and measured travel path is less than 5% (Zhao, 2016). Temperature data for each girder is taken from a temperature sensors installed between each girder and concrete. The dummy variable for the frozen ground is equal to unity if the average temperature is below 0 °C for more than the two previous weeks, because it is assumed that the frozen ground takes two weeks to thaw. The length of the freeze and thaw processes are assumed to be two weeks because the soil under the piers is mostly clay, which takes longer than sand to freeze and thaw. The duration of the freeze and thaw processes can be adjusted if additional soil properties are available for the site.

The regression analysis was performed with Minitab (2014), a statistic analysis program, and the regression results are shown in Table 2. All models have high values of adjusted R^2, a goodness-of-fit measure which implies that the overall variations of the GDFs are well-approximated by the selected models. The adjusted R^2 for girder 3 is not as high as other girders. The reason could be that the 3rd order polynomials used do not fully

capture the relationship between travel path and the GDF of girder 3. The p-values of the predictors for girder 5 indicate that the model coefficient for temperature is not statistically significantly different from zero. However, this p-value is high because the numerical value of the coefficient for temperature predictor is effectively very close to zero, leading to very low t-ratio. Since the other five girders demonstrated temperature sensitivities, the temperature predictors for all girders are kept in the model. From Table 2, it can be concluded that the GDF regression models exhibit excellent overall goodness of fit between the GDF observations and model predictions based on the predictors included.

Table 2. GDF Regression Model Summary

		Regression Terms							Adj. R^2
		Constant	Bridge Age	Temp.	Frozen	Travel Path	Travel Path square	Travel Path cubic	
G1	β	5.13E-1	-1.12E-2	3.05E-4	3.84E-3	-1.97E-1	2.58E-2	-1.26E-3	97.76%
	p-value	0.00	0.00	0.00	0.00	0.00	0.00	0.00	
G2	β	4.74E-1	8.35E-3	-3.29E-4	-2.45E-3	3.15E-2	-2.48E-2	1.97E-3	99.32%
	p-value	0.00	0.00	0.00	0.00	0.00	0.00	0.00	
G3	β	-1.83E-1	4.52E-3	1.39E-4	-2.17E-3	2.32E-1	-3.54E-2	1.29E-3	92.83%
	p-value	0.00	0.00	0.00	0.00	0.00	0.00	0.00	
G4	β	2.69E-1	1.64E-3	-8.60E-5	-1.15E-3	-1.39E-1	4.40E-2	-3.32E-3	99.46%
	p-value	0.00	0.00	0.00	0.00	0.00	0.00	0.00	
G5	β	-3.99E-2	-8.80E-4	2.02E-6	1.18E-3	4.63E-2	-6.66E-3	8.40E-4	99.62%
	p-value	0.00	0.00	**0.86**	0.00	0.00	0.00	0.00	
G6	β	-3.52E-2	-2.37E-3	-2.35E-5	7.56E-4	2.56E-2	-2.96E-3	4.86E-4	99.48%
	p-value	0.00	0.00	0.03	0.00	0.00	0.00	0.00	

As discussed earlier, the multiple regression uses OLS to calculate the model coefficients. Though it is important to evaluate the behavior of the model residuals to

properly interpret the statistical significance of the model coefficients, it should be highlighted here that the regression models of the six girders display a very high level of goodness of fit, as evidenced by the very high values of R^2.

Rigorous evaluations of the model residuals are performed to determine if the usual assumptions of normality, homoscedasticity and independence held. The residuals are found to be approximately normally distributed, exhibit relatively constant variance, and are approximately independent of time in most cases. Such evaluations are extremely important if one wishes to improve the model, because the residuals contain information about the unknown, providing insight into how the model could be improved. Normally residual evaluations are also performed to ensure that the statistical inferences of the model parameters, such as computing p-values and other hypothesis tests concerning the model, are sensible. In this case, the goal is to maximize the overall goodness of fit of the model to ensure that the residual errors only contained information concerning bridge damage, and thus are not impacted by other environmental conditions such as temperature or bridge usage. Instead, a rigorous evaluation of the resulting model is performed in the next section to test the ability of the model residuals to describe the likelihood of potential bridge damage. Thus, when p-values of the model coefficients are reported, they are only approximate values, which are indicative of the degree to which an explanatory variable belongs in the model. That is, a low p-value indicates a low probability that the corresponding model coefficient is equal to zero and thus should be included in the resulting model. However, the existing model captured nearly all the observed variations of the GDFs with the available data. The detrended GDF ranges are much smaller than the ranges of the original GDFs, and the distribution of detrended GDFs are more normal than the original GDFs, thus showing that the accuracy of identifying bridge damages is improved by detrending the GDFs.

3.4.6 Detrending the distributions of the GDFs

The goal of building multiple regression models for GDFs is to remove the effects of deterioration, temperature, frozen ground, and vehicle travel path on the behaviors of the GDFs, leaving the GDFs to be affected by only structural factors. GDFs values with the removal of the effects of these values on them is termed detrended GDFs. Once the regression models are validated, the GDFs can be detrended so that the detrended GDFs become independent of the predictors. The detrended GDFs are calculated by removing the variation of non-structural factors, as shown in (22).

$$Detrended\ GDF = GDF - \boldsymbol{\beta}^{\bullet}(\mathbf{X}_{measured} - \mathbf{X}_{baseline}) \tag{22}$$

where $\boldsymbol{\beta}$ is the vector that contains the regression coefficients of the non-structural factors. $\mathbf{X}_{measured}$ and $\mathbf{X}_{baseline}$ are the vectors that contain the measured and baseline values of non-structural variables, respectively. A baseline configuration is used rather than deleting the non-structural terms from the GDFs. Deleting the non-structural terms does not always make sense because some parameter values cannot have zero values. For example, a travel path having a value of zero means a vehicle's centerline is on the southbound curb, which is not feasible. In this research, the baseline non-structural parameter values used are a one-year-old bridge at 20°C with unfrozen ground and a travel path of 3 meters. These are typical values, and although other parameter values can also be used, the capability of damage detection will be the same regardless because all the non-structural variables are set to be a meaningful constant value.

The calibrated model captured nearly all the observed variations of the GDFs with the available data. To compare the distributions of GDFs and detrended GDFs, boxplots are plotted in Fig. 27. A boxplot is a nonparametric depiction of the cumulative distribution of a random variable. In the boxplot, the rectangle represents the distribution from first quartile to third quartile, which is often referred to as the interquartile range (IQR); the line

in the box shows the value of median; outliers are defined as more than three times the IQR above third quartile or below the first quartile. By comparing the variability in panels (a) and (b) in Fig. 27, it should be noted that the range of the detrended GDFs are much smaller than the ranges of the original GDFs. This indicates the ability of the regression model to remove the effects of the various environmental variables considered. In addition, the distribution of detrended GDFs are more normally distributed than the original GDFs. It can be concluded that the regression model is useful for removing the environmental factors and traffic event factors from the GDFs. The detrended GDFs preserve the feature that the sum of GDFs from all six girders equals to one, denoting that the girders are carrying 100% of the applied gravity live loads. This feature ensures that the detrended GDFs still represent the peak strains relative to other peak strains for the same environmental conditions and travel path.

The detrended GDFs are uncorrelated with all predictors because the predictors are replaced with predefined constant values. To evaluate the correlation between the GDFs and various predictors, the relationships between vehicle travel path and detrended GDFs are plotted in Fig. 28. The detrended GDFs are independent of vehicle travel path, which indicates that the transverse location of the vehicle does not affect the detrended GDFs and that traffic events from all traffic lanes can be used to detect damages. Similarly, since detrended GDFs are independent of temperature and frozen ground, traffic events from all seasons can be used to detect damage. It is important to note that all the single-vehicle traffic events collected can be used to detect damage by using the detrended GDFs as the index.

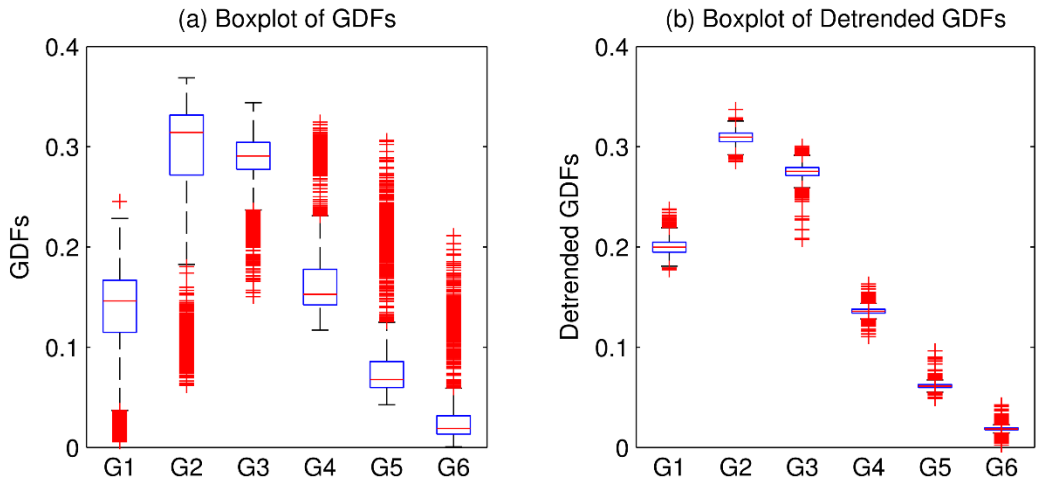

Fig. 27: Boxplot for (a) GDFs and (b) Detrended GDFs

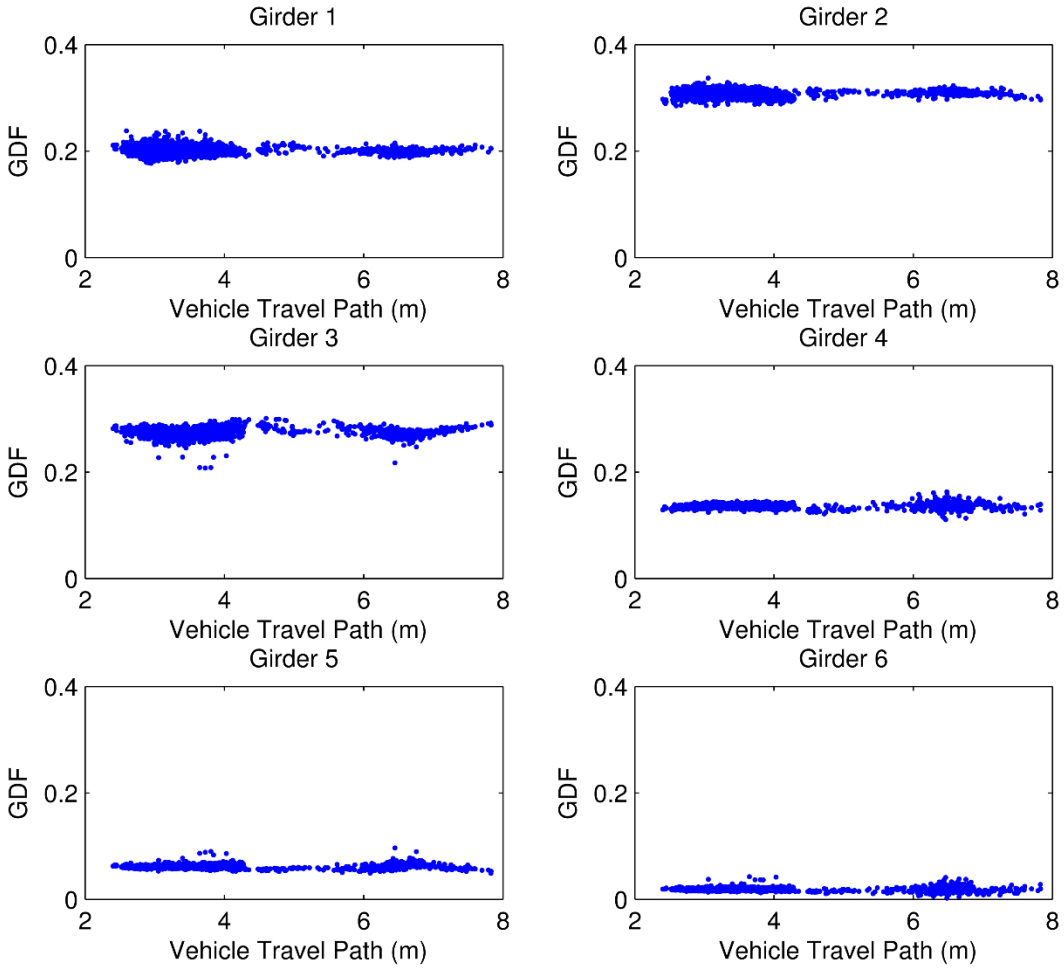

Fig. 28: Relationship between Vehicle Travel Path and Detrended GDFs for All Girders

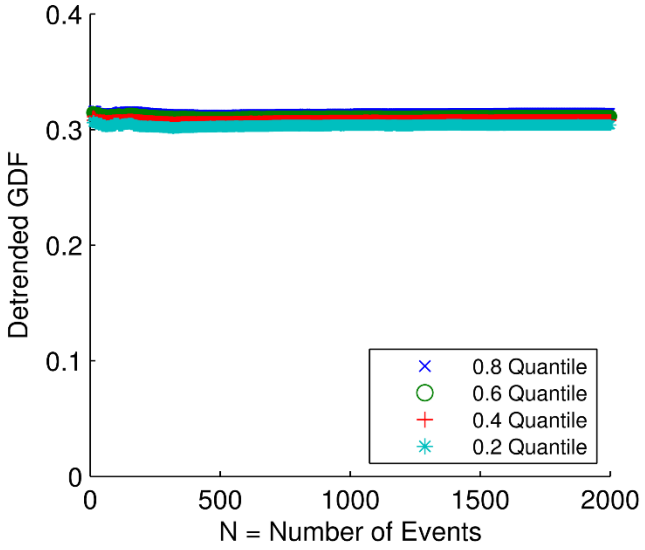

Fig. 29: Quantile Plot of Detrended GDF of Girder 2

After the detrending of the GDFs, the quantile plot of the detrended GDF of girder 2 is plotted in Fig. 29, which illustrates that the ranges of the detrended GDFs are significantly lower than the ranges of the original GDFs of the observations in Fig. 25 and that the distributions of detrended GDFs are now stable, unlike the somewhat unstable previous results in Fig. 25. The boxplot of GDFs and the boxplot of detrended GDFs are also compared in Fig. 27, which indicates that the distributions of detrended GDFs are much more concentrated and centralized than the distributions of the original GDFs. It is also important to note that using the detrended GDFs instead of the original GDFs improves the accuracy of the GDFs and the minimum damage detection level.

Considering the benefits of increasing the amount of usable traffic events by collecting in all four seasons and improving the minimum damage detection level and accuracy, the detrended GDFs are an excellent index for damage detection compared to the original GDFs.

3.5 Statistical Analysis for Damage Detection and Localization

Rytter (1993) introduced the four stages of damage identification as detection, location, quantification, and prognosis. The proposed method enables the first two stages

by utilizing the following two statistical methods: (1) the Wilcoxon rank-sum test to detect any change in the distribution of detrended GDFs for newly collected truck event data, and (2) the bootstrap method to construct bridge signatures to locate the potential damage. The nonparametric Wilcoxon rank-sum test can detect a change in detrended GDFs for any defined significance level. Any statistically significant change in the detrended GDF may be considered as demonstration of potential bridge damage. The 95% tolerance interval of detrended GDFs is obtained from the bootstrap method. The detrended GDFs from a damaged bridge can be plotted with the 95% tolerance interval of the healthy bridge to locate the potential damage and assess the severity of that potential damage.

3.5.1 Damage Detection

In practice, the proposed method does not require the use of a finite element model (FEM) to analyze the bridge response and assess the bridge health condition. However, since the bridge is not damaged, a tool is needed to simulate damage to test the proposed method. Reiff et al. (2016) proposed the of a calibrated FEM developed by Sanayei et. al (2012) to simulated the damage and response. They defined the undamaged bridge as Case U, and four different typical damage cases: (A) interior girder fracture, (B) exterior girder Corrosion, (C) diaphragm fracture, and (D) deck delamination. These damage simulations were based on actual bridge damage investigations that were summarized by Reiff et al. (2016). The GDFs were calculated from the simulated strain response of FE model for an HS-20 truck crossing the bridge with constant speed on the southbound lane. The differences between simulated GDFs from a damaged case and the undamaged case are defined as ΔGDFs for a given simulated damage case. Since girder 6 is away from southbound lane and did not produce large strains, the change in GDF for girder 6 is zero. It is assumed that the GDFs for the damaged case are equal to the observed GDFs (based on measurements) plus ΔGDFs. In this research, the concept and ΔGDFs are adopted to

evaluate the proposed method. The ΔGDF represents some change in the live load distribution that is possibly due to damage. The changes are added to the measured detrended GDFs and then compared to baseline sample to verify that the proposed statistical framework is capable of detecting changes in GDFs.

		Truth	
		H_0 Bridge is Not Damaged	**H_A** Bridge is Damaged
Decision	Conclude Bridge is Not Damaged	No Error $1 - \alpha$ (No Damage)	Type II Error β (Under-preparedness)
	Conclude Bridge is Damaged	Type I Error α (Over-preparedness)	No Error $1 - \beta$ (Damage)

Fig. 30: Damage Detection Hypothesis Test Decision Matrix

The Wilcoxon rank-sum test has been widely adopted as a nonparametric approach to detect the difference between two sets of samples (Wilcoxon, 1945). The Wilcoxon rank-sum test is a nonparametric hypothesis test which determines whether the two samples arise from the same distribution at a defined significance level. In the proposed method, the most recently collected 50 events, which is approximately the average number of usable single-vehicle events collected in a week, are considered as a sample. All 2259 collected events are considered as the base set. The Wilcoxon rank-sum test is performed between detrended GDFs from the recent set of samples and the base set with a given significance level. Fig. 30 shows the decision matrix for the damage detection hypothesis, which was originally developed by Reiff et. al (2016). As shown in Fig. 30, there are two types of errors presented. Type I errors result from concluding a healthy bridge damaged, leading to over-preparedness. Type II errors result from concluding a damaged bridge healthy, leading to under-preparedness. The significance level also corresponds to the probability of a Type I

error for individual girders. The outcome variable from the rank-sum test, *h*, is a binary variable equal to 0 or 1, with a value of unity implying that the recent set is different from the base set. These binary outcome variables of the rank-sum test are used to construct a bridge Damage Index (DI) as (23) (Reiff et. al, 2016)

$$DI = \frac{\sum_{i=1}^{N} h_i}{N} \tag{23}$$

The DI can be interpreted as the average number of sets that are different from the base set expressed as a fraction of the overall number of sets considered.

To evaluate the capabilities of the proposed method, an experiment is performed by simulating 10000 trials for five different cases. Case U is the undamaged bridge case. Cases A, B, C, and D are girder 2 fracture, girder 1 corrosion, diaphragm cracking, and deck delamination, respectively. The outcomes from the simulated experiments with a significance level equal to 5% are summarized in Fig. 31. The y-axis illustrates the percentage of trials that resulted in DI values that are equal to or larger than the corresponding DI values given on the x-axis. As expected, when the damage index is zero, no damage was detected, and similarly when the damage index is unity, damaged girders were always detected. Since there is no damage added to girder 6, the theoretically highest DI value in the simulation is 5/6. Some cases with a small percentage of trials resulted in DI values of unity due to the occurrence of a Type I error for girder 6. The overall probabilities of Type I errors and Type II errors are more important to evaluate in this research, which can be read in Fig. 31. A Type I error is defined as having at least one of the six girders with detrended GDFs result in a GDF distribution that is different from the GDF distribution of the base set for an undamaged bridge. The overall Type II error is defined as having all the girders with detrended GDFs having the same detrended GDF distributions as the base set for a damaged bridge. For the undamaged case, 18.9% of the

trials have DI values larger than zero, which is a measure of the overall likelihood of a Type I error across all trials. For the damaged cases, 100% of the trials have DI values larger than zero, which implies that all the damaged cases are identified, thus the overall likelihood of a Type II error is less than 0.01% for the 10,000 trial simulations considered. For all damaged cases, 100% of trials have DI values that are equal or larger than 3/6, which means at least three girders can be identified as damaged for all the scenarios considered.

Although the likelihood of Type I errors is high in the simulations, the type I error can be reduced by setting a lower significance level in the rank-sum test. In Fig. 32, the simulation trials are performed with significance level equal to 0.1%. In this simulation, lowering the significance level does reduce the capability to detect damage, which is illustrated by comparing the results in Fig. 31 and Fig. 32 with high DI values. Nevertheless, the overall Type II error is still less than 0.01% for the 10,000 trials considered and the overall Type I error for this case dropped significantly. From the simulated experiments, the proposed method illustrates that the proposed approach, which is based on detecting damage using changes in the detrended GDFs, was found to be very effective for detection of damage and simultaneously led to a very low probability of false damage alarms.

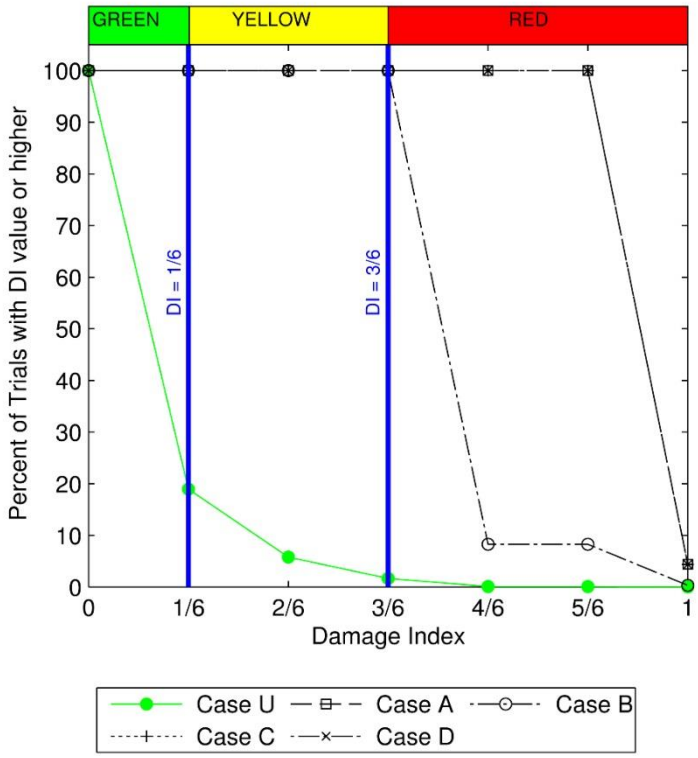

Fig. 31: Damage Detection Rate from 10000 Trials with α=5%

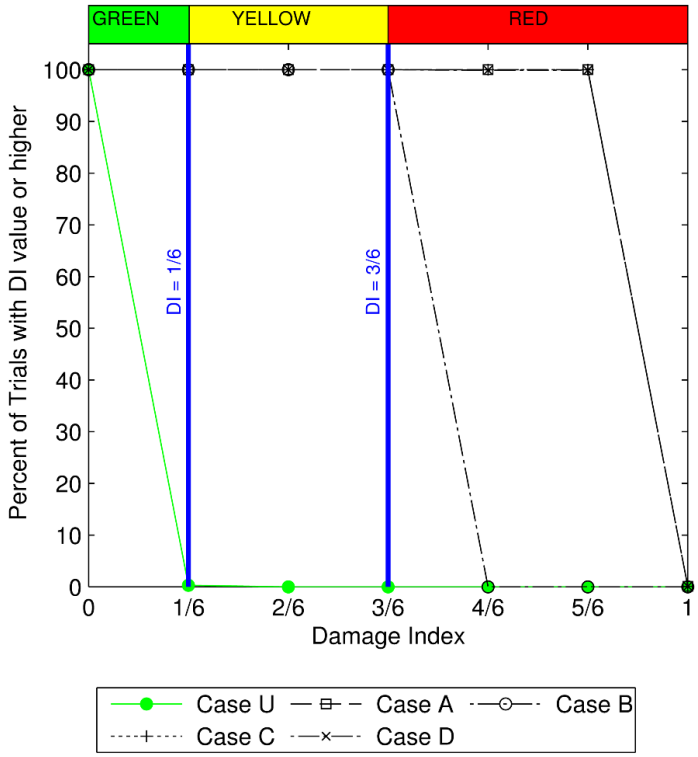

Fig. 32: Damage Detection Rate from 10000 Trials with α=0.1%

The term power is defined as the probability of not making a type II error, thus it is a measure of the likelihood to detect a damaged bridge when it is truly damaged. In Fig. 32, for cases with significant damage, such as Case A, the power of the test is high for all DI values. Cases with relatively small damage, such as Case B, can only be identified for the girders that are physically close to damaged bridge sections, where the DI values are not as high as for the significantly damaged cases. The thresholds between healthy condition, damaged condition, and significantly damaged condition are determined at 1/6 and 3/6, which is consistent with previous research by Reiff et. al, (2016). The Red, Yellow, and Green conditions are used to make recommendations for inspections. For a new set of traffic events, the DI value and thresholds are used for future condition assessment decisions. A healthy bridge shall have a DI value equal to or near zero. A severely damaged bridge will have a DI value that equals or exceeds 3/6, which means at least half of the girders are damaged. The DI provides a quantitative measure that can be used to provide warnings of the likelihood of potential damage. However, the damage index does not have the ability to determine the location of the potential damage.

3.5.2 Damage Localization

A Bridge signature introduced by Follen et al. (2014) is another tool that can be used to assess bridge health condition by predicting the possible location of the damage. Bridge Signatures are developed with a nonparametric empirical cumulative probability distribution for the detrended GDFs. The Bootstrap method, which is a generalized resampling approach, is used to construct the bridge signature. Each bootstrap sample is chosen randomly, with replacement, from the baseline set of GDF measurements. Here the sample size is assumed to be 50 events. Follen et al. (2014) found that the bridge signature is stable after roughly 1000 resampling experiments. The bootstrap resampling procedure is repeated 1000 times, creating 1000 samples of 50 events. In each sample, the 50 events

are sorted in ascending order. At each rank, the largest 2.5% and the smallest 2.5% of the 1000 samples are removed to create a 95% tolerance interval. 95% of the healthy bridge signature will fall within this envelope.

The resulting baseline bridge signatures envelope for girder 1 with healthy and damaged sets are shown in Fig. 33. The thick dark green lines are the bridge signature envelope. The thin light green line is the set of traffic events from a healthy bridge. The orange dashed line is the set from damaged cases. Areas in which the girder signature is outside the confidence interval indicate some form of structural change or damage. If the girder signature is above the envelope, that girder is receiving additional load from adjacent possibly damaged girders. If the girder signature is below the envelope, that girder has lost some capability to carry loads. For Cases A and B, the damaged sets are significantly further outside of the bridge signature envelope than are Cases C and D. This indicates that the damage in Cases A and B are most probably at girder 1, or high in magnitude and near girder 1. It also can be seen that the damaged set for Case A is above the envelope. Having higher detrended GDFs than the envelope indicates that the adjacent girder has damages. For Cases B, C, and D, having lower detrended GDFs than the envelope might be a sign that girder 1 has damage that reduces its load-carrying capability.

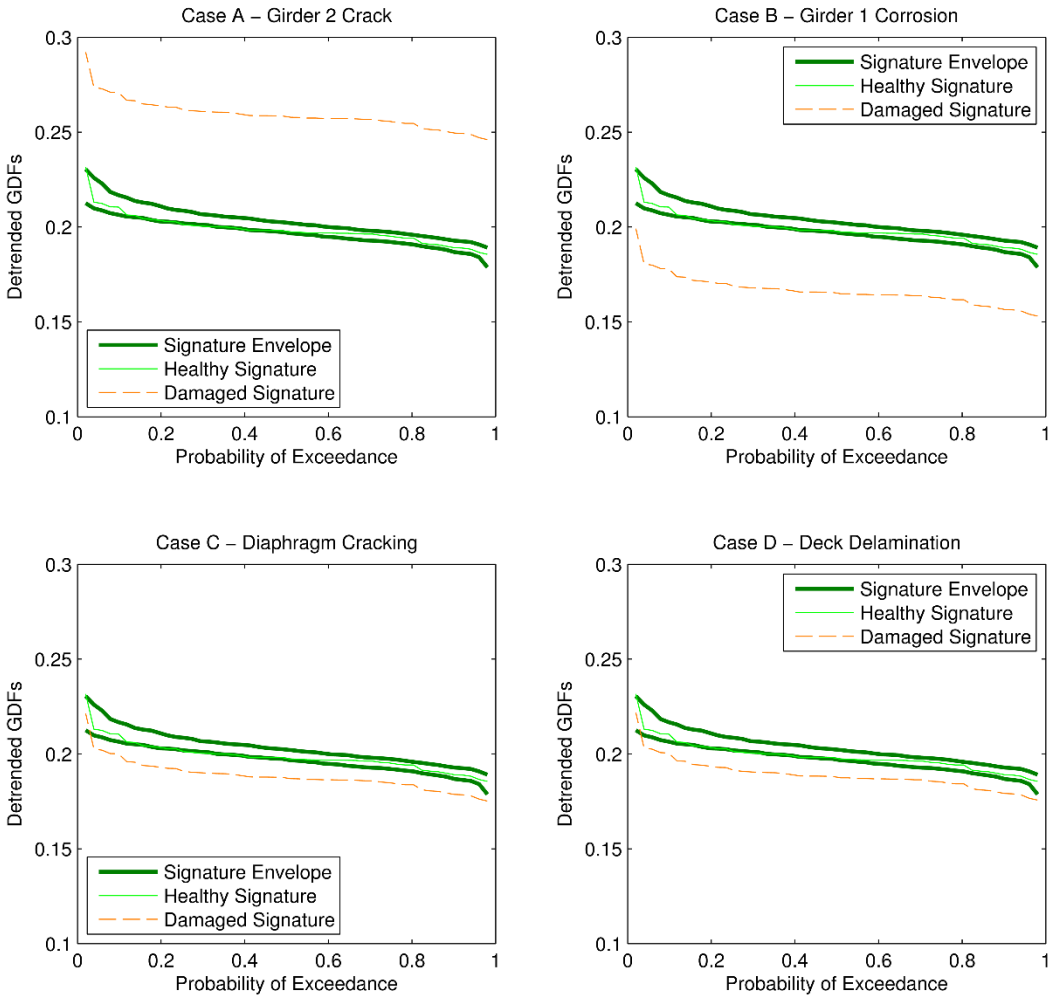

Fig. 33: Bridge Signature Envelope for Girder 1

Envelopes corresponding to the sets of bridge signatures for all girders are combined in a 3D plot to create a bridge signature surface. Fig. 34 shows the bridge signature surface with a 95% confidence interval in dark green and the damage surface in orange. Areas in which the damage surface is outside of the confidence interval indicate some form of structural change or damage. From the figure, Case A has the largest magnitude of damage and the magnitude of girder 2 dropped significantly, which indicates girder 2 might be significantly damaged. The lower damage surface at girder 1 in Case B indicates that there might be damage on girder 1. Cases C and D have less damage and

there is no significant drop of the damage surface, which means that the damage is not on the girders but rather another structural component of the bridge. If the damage is near the location a strain gauge, it is easy to detect the damage. The damage cannot be detected when the sensors are far away from the damage location. The proposed method is more powerful to detect damage on girders rather than other structural components because the strain gages were located on the bottom flange of girders at midspan.

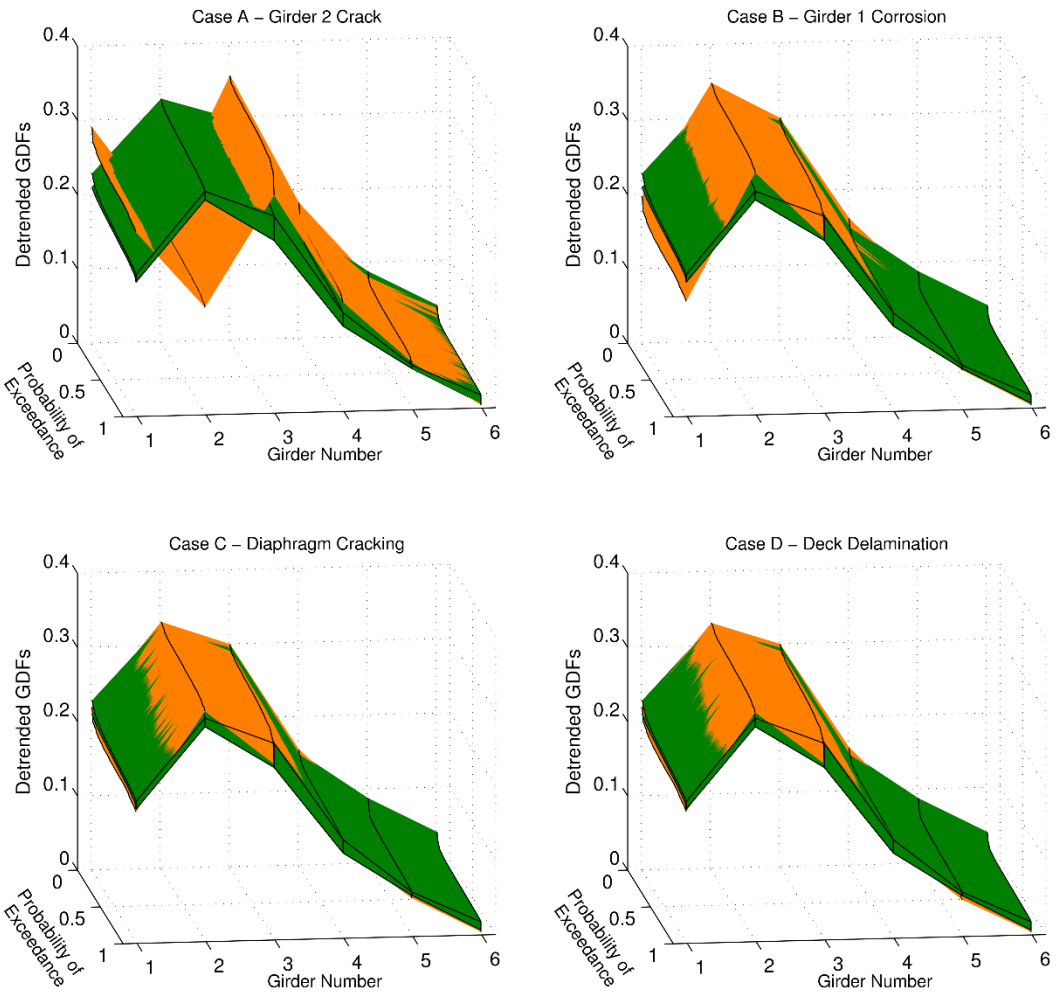

Fig. 34: Bridge Signature surface of Detrended GDFs

3.6 Discussion

There are many variables that may influence GDFs and resulting bridge responses. During the process of creating the multivariate regression model, many assumptions were made to simplify the modeling. Though more complex models of the GDF may be considered, this initial study indicates that most of the variation of GDFs is captured by the multivariate model and the proposed method is shown to be effective for detection of damage, while maintaining a low probability of false damage alerts in our artificial simulation experiments.

Instead of waiting for regularly scheduled bi-annual visual inspections resulting in decisions about bridge load posting, closure, and repair, the proposed method can monitor the response and alert the bridge owners and managers based on real-time changes in bridge's response to traffic events. The proposed method can be considered as a supplement to visual inspections, where early detection in change in GDFs distributions can trigger visual inspections.

3.7 Conclusions

Previous research has shown that bridge Girder Distribution Factors can be effective indicators of bridge damage using operational measured strains. It has been demonstrated that the development of a multivariate regression model is a powerful tool to quantify the factors that affect bridge GDFs. Bridge age, temperature, frozen ground, and vehicle travel path were found to all be related to GDFs in statistically significant ways. The resulting model enabled us to remove variations of GDFs caused by environmental factors and traffic events, resulting in detrended GDF's which were independent of those factors. A nonparametric rank-sum test was used to identify statistically significant changes in detrended GDFs to detect damages. The nonparametric Bootstrap method was then used to build bridge signatures to assess the locations of damages. A baseline sample of

detrended GDFs was collected from measured long-term traffic events. A simulated hypothesis test showed that bridge damage could be detected in a meaningful fashion using detrended GDFs. The proposed method was shown to exhibit high statistical power that is a high likelihood of detecting damage when it is present as well as a low probability of issuing false damage alerts. The proposed operational, non-parametric, and non-FEM-based method using only measured strains is highly computing-efficient and can be used for real-time monitoring of bridges for condition assessment.

3.8 Future Works

This proposed method focuses on detecting bridge damages from single vehicle traffic events based on detrended measured GDFs. For many busy bridges, it may be difficult to record single-vehicle traffic events. For many wide bridges that contain multiple traffic lanes in each direction, GDFs for girders that are far away from traffic may have low signal to noise ratios. Future research using the proposed methodology could be used to determine the location of the damage in both transverse direction and longitudinal direction. In addition, this initial study only applied our methodology to one bridge. Additional research is needed to investigate the applicability of our approach to longer-span bridges, wider bridges, and other bridge types. For future studies, researchers can apply the proposed concept of multivariate regression to other damage indicators to remove the non-structural effects.

3.9 References

Alampalli, S. (2000). Effects of testing, analysis, damage, and environment on modal parameters. *Mechanical Systems and Signal Processing, 14*(1), 63-74.

Bishara, A. G., Liu, M. C., & El-Ali, N. D. (1993). Wheel load distribution on simply supported skew I-beam composite bridges. *Journal of Structural Engineering, 119*(2), 399-419.

Busa, G. D., Cassella, M. A., Gazda, W., & Horn, R. J. (1985). *A national bridge deterioration model* (Staff Study No. SS-42-U5-26). Transportation Systems Center, Cambridge, MA: U.S. Department of Transportation.

Cardini, A. J., & DeWolf, J. T. (2008). Long-term structural health monitoring of a multi-girder steel composite bridge using strain data. *Structural Health Monitoring*.

Chen, C., & Johnston, D. W. (1987). Bridge management under a level of service concept providing optimum improvement action, time, and budget prediction *(Final Report No. FHWA/NC/88-004). Raleigh: Center for Transportation Engineering Studies, North Carolina State University*.

Comanducci, G., Magalhães, F., Ubertini, F., & Cunha, Á. (2016). On vibration-based damage detection by multivariate statistical techniques: Application to a long-span arch bridge. *Structural Health Monitoring*, 1475921716650630.

Draper, N. R., & Smith, H. (2014). *Applied regression analysis*. John Wiley & Sons.

Eamon, C. D., & Nowak, A. S. (2002). Effects of edge-stiffening elements and diaphragms on bridge resistance and load distribution. Journal of Bridge Engineering, 7(5), 258-266.

Enright, M. P., & Frangopol, D. M. (1999). Reliability-based condition assessment of deteriorating concrete bridges considering load redistribution. *Structural Safety*, *21*(2), 159-195.

Eom, J., & Nowak, A. S. (2001). Live load distribution for steel girder bridges. *Journal of Bridge Engineering*, *6*(6), 489-497.

Federal Highway Administration. (2004). "National Bridge Inspection Standards." 23 CFR Part 650.

Federal Highway Administration. (2011). "Traffic Volume Trends." www.fhwa.dot.gov.

Follen, C. W., Sanayei, M., Brenner, B. R., & Vogel, R. M. (2014). Statistical bridge signatures. *Journal of Bridge Engineering*, *19*(7), 04014022.

Frangopol, D. M., Lin, K. Y., & Estes, A. C. (1997). Life-cycle cost design of deteriorating structures. Journal of Structural Engineering, 123(10), 1390-1401.

Goyal, R., Whelan, M. J., & Cavalline, T. L. (2016): Characterising the effect of external factors on deterioration rates of bridge components using multivariate proportional hazards regression, Structure and Infrastructure Engineering, DOI: 10.1080/15732479.2016.1217888

Guan, H., & Karbhari, V. M. (2008). Vibration-Based Structural Health Monitoring of Highway Bridges (No. CA06-0081).

Jin, C., Li, J., Jang, S., Sun, X., & Christenson, R. (2015, March). Structural damage detection for in-service highway bridge under operational and environmental variability. In *SPIE Smart Structures and Materials+ Nondestructive Evaluation and Health Monitoring* (pp. 94353A-94353A). International Society for Optics and Photonics.

Kim, Y. J., Green, M. F., & Wight, R. G. (2008). Live load distributions on an impact-damaged prestressed concrete girder bridge repaired using prestressed CFRP sheets. *Journal of Bridge Engineering*, *13*(2), 202-210.

Kromanis, R., & Kripakaran, P. (2014). Predicting thermal response of bridges using regression models derived from measurement histories. *Computers & Structures*, *136*, 64-77.

Madanat, S., & Ibrahim, W. H. W. (1995). Poisson regression models of infrastructure transition probabilities. *Journal of Transportation Engineering*, *121*, 267–272.

Madanat, S., Mishalani, R., & Ibrahim, W. H. W. (1995). Estimation of infrastructure transition probabilities from condition rating data. *Journal of Infrastructure Systems, 1*, 120–125.

Mašović, S., Hajdin, R. (2014) Modelling of bridge elements deterioration for Serbian bridge inventory, Structure and Infrastructure Engineering, 10:8, 976-987, DOI: 10.1080/15732479.2013.774426

Minitab, I. (2014). MINITAB statistical software. Minitab Release, 17.

Moore, M., B. Phares, B. Graybeal, D. Rolander, and G. Washer. (2001). Reliability of Visual Inspection for Highway Bridges: Federal Highway Administration.

National Snow and Ice Data Center (NSIDC). (2016) *How Does Frozen Ground Form?* https://nsidc.org/cryosphere/frozenground/how_fg_forms.html Accessed 16 Oct. 2016.

Nowak, A. S., & Hong, Y. K. (1991). Bridge live-load models. *Journal of Structural Engineering*, *117*(9), 2757-2767.

Plude, S. (2011). Implementing a long-term bridge monitoring strategy for a composite steel girder bridge.

Rytter, A. (1993) Vibration based inspection of civil engineering structures. Ph.D. dissertation, Aalborg University, Denmark.

Reiff, A. J., Sanayei, M., & Vogel, R. M. (2016). Statistical bridge damage detection using girder distribution factors. *Engineering Structures*, *109*, 139-151.

Sanayei, M., Phelps, J. E., Sipple, J. D., Bell, E. S., & Brenner, B. R. (2012). Instrumentation, nondestructive testing, and finite-element model updating for bridge evaluation using strain measurements. *Journal of bridge engineering*, *17*(1), 130-138.

Stanton, John F., Charles W. Roeder, and T. Ivan Campbell. (1999). *High-load multi-rotational bridge bearings*. No. 432. Transportation Research Board, 1999.

Stanton, John F., and Charles W. Roeder. "Elastomeric bearings design, construction, and materials." *NCHRP report* 248 (1982).

Tabsh, S. W., & Tabatabai, M. (2001). Live load distribution in girder bridges subject to oversized trucks. *Journal of Bridge Engineering*, *6*(1), 9-16.

U.S. Department of Transportation (2015). Highway statistics. Retrieved from http://www.fhwa.dot.gov/bridge/structyr.cfm

Whelan, M. J., & Gangone, M. V. (2015). Effect of measurement uncertainties on strain-based damage diagnostics for highway bridges. *Journal of Civil Structural Health Monitoring*, *5*(3), 321-335.

Wilcoxon, Frank. (1945). "Individual Comparisons by Ranking Methods." Biometrics Bulletin 1 (6): 80-83.

Wipf, T. J., Phares, B. M., Greimann, L. F., Hemphill, D., Doornink, J. D., & Lu, P. (2006). *Remote continuous evaluation of a bridge constructed using high-performance steel* (No. CTRE Project 02-123).

Zhao, Zhiyong. (2016). Cloud-based Real-time Continuous Bridge Monitoring: Bridge Weigh in Motion and Condition Assessment. *M.S. Thesis*, Tufts University.

Chapter 4
Cloud-based Real-time Continuous Bridge Monitoring for Condition Assessment

4.1 Abstract

Current bridge inspection routine relies on visual inspection by inspectors visiting the bridge every two years required by Federal Highway Administration. The proposed system provides an automated measurement-based objective evaluation of bridge performance with 24/7 monitoring capability. To prove the concept, a prototype of the system was developed using Microsoft Azure Virtual Machine (VM) and two lab computers. One of the computers acts as fully instrumented bridge that can record the strain response of heavy vehicle traffic events, preliminarily process the recordings, and transfer the traffic events to the cloud-computing hub. The VM is acting as cloud-computing hub where traffic events are processed and stored for hypothesis testing and bridge condition assessment. The bridge performance recommendations are published on a website that is also hosted on the VM. The other computer acts as the Bridge Health Portal that grants the access for bridge engineers and the structure owners from any remote location. The proposed system adopted hypothesis testing framework and bridge signatures using detrended Girder Distribution Factors for bridge condition assessment. The information security, responsibility, liability, capabilities, and limitations related to the real-time continuous bridge monitoring for condition assessment is also discussed.

4.2 Introduction

From the car tire pressures to offshore oil platforms, many important objects are being continuously monitored for safety, performance assessment, emergency response, and maintenance planning. In Civil Engineering field, continuous monitoring can be applied to key infrastructures and structures such as bridges, buildings, dams, wind turbines, transmission towers, offshore platforms, or other constructed facilities. The structures can be closely monitored for accessing their structural conditions under short-term and long-

term threats. The collected measurements from sensor system due to the threat event are only useful if it can be processed and translated to meaningful feedbacks on time. Real-time continuous monitoring employs near real-time data transition and rapid condition assessment to achieve real-time condition assessments and recommendations. The collected measurements are transferred to computation module and are analyzed by automated programs to give recommendations at the minutes the event occurs. Such analysis can be done at an onsite computation module. However, cloud-based computing has the following advantages compared to on-site computing: (1) it provides more reliable and faster computation system, (2) the possibility of service interruptions is low, (3) data integrity is protected by reliable backups for disaster recovery, (4) the computation capabilities are adjustable, (5) deployment and configuration are simple and standardized, and (6) the data can be easily accessed. Cloud-based real-time continuous monitoring can be applied to many types of structures for different purposes and with different decision algorithms. The proposed system here is applied to bridge condition assessment and utilizing a detrended measured Girder Distribution Factors (GDFs) method for continuous watching for any structural changes and for any potential damage.

Structural Health Monitoring (SHM) has developed significantly in the past decades. One of the key purposes of SHM is to detect structural damages. Many methods and frameworks were developed using different methods of measurements. There are many types of data that can be monitored for a bridge, including acceleration, displacement, tilt angle, and strain. Doebling et al. (1996) conducted a literature review of SHM and damage detection techniques based on vibration measurements. Farrar and Worden (2012) studies SHM from a machine learning perspective utilizing statistical pattern recognition. Sartor et al. (1999) discussed the savings in the costs and time using SHM systems, noting that short-term monitoring can provide accurate insight into structural behavior and help bridge

owners planning rehabilitation when it is necessary. Li et al. (2016) reported the state-of-the-art in SHM for large civil infrastructures.

For real-time bridge monitoring, many researchers have conduct studies utilizing different methodology recently. Yang (2015) proposed an SHM system that can identify real-time bridge status for remote cold regions. Al-Radaideh et al. (2015) designed a system that can monitor different types of sensors through wireless data acquisition units on highway bridges and determine bridge condition through a fuzzy logic. Malekzadeh et al. (2015) introduced a hybrid data interpretation framework for long-term real-time structural performance assessment by integrating parametric and non-parametric approaches.

In reality, real-time computing cannot be instantaneous due to the required computing time. In this study, bridge condition assessment using strain measurements can be done within seconds. Transmission of this intermittent and small packet of data to the secure cloud-based computing hub will be nearly instantaneous using wired or wireless internet connections. After data transmission, the cloud computing hub will perform a hypothesis test on a last-in-first-out basis, which requires relatively little computation time. At the same time the cloud computing hub can process many bridges at the same time and report to the corresponding bridge owners and managers. There can be challenges involved in this process such as communication bandwidth limitations, compatibility of devices, and computing efficiency that can be overcome by careful planning. The goal of this study is to make the near real-time continuous system as fast as possible.

The proposed system has some capabilities that can result in advantages compared to conventional bridge condition assessment. There are also some limitations of the proposed system, which leads to disadvantages. The capabilities and limitation of the proposed system as well as the advantages and disadvantages are summarized in Table 3.

Table 3. Capability and Limitations of Proposed System

Capabilities	Advantages
1. Measurements are from girder strain gauges	➢ Direct access to stiffness of bridge girders ➢ Objective bridge evaluation
2. Fast computing	➢ Real-time evaluations and recommendations
3. Continuous monitoring	➢ Recommendations for early bridge inspections ➢ A safer system throughout the years
4. Observation of changes in inaccessible areas	➢ More reliable assessment of bridge conditions
5. Bridge engineers/managers set bridges inspection trigger levels	➢ Full control on the thresholds for decision-making
6. Bridge database/history	➢ Future objective analysis/study
7. Low cost system	➢ The cloud computing system can monitor many bridges simultaneously
Limitations	**Disadvantages**
1. Requires some level of bridge instrumentation and computing	➢ Some cost and effort per bridge
2. Requires bridge signature recordings	➢ Requires single heavy vehicles events to establish the GDFs' signature. ➢ In this case, the number of events was 1000. The number of days depends on bridge traffic

Among these advantages, the real-time recommendation based on objective measurements of girder components make the proposed system appealing compared to conventional bridge condition assessment methods. Other advantages, such as bridge damage detection at early stages and inaccessible area, the owner-controlled threshold for decision-making, and complete bridge database that can be used, leading to an even more robust system.

The limitations and disadvantages of the proposed system are inevitable because extra efforts are needed to obtain the additional information about the bridge health conditions. However, the real-time bridge condition assessment can reduce overall cost by detecting the damage in early stage and helping human inspectors to locate the damage,

even in inaccessible areas. The required cost and effort in the proposed system is relatively small because only strain gauges and temperature sensors are needed, and there is no need for bridge closures. The cloud computing system can easily monitor many bridges simultaneously using different damage thresholds set by bridge engineers and managers. Economic analysis can be performed on the extra cost and effort due to the proposed system and the benefits and cost savings that the system can provide.

4.3 Data and Software

The strain measurements from heavy trucks crossing Powder Mill Bridge (PMB) are used in this research. PMB is a three-span steel girder bridge in Barre, Massachusetts as shown in Fig. 35. Six steel plate girders are in composite action with a reinforced concrete deck. The bridge carries a two-way traffic with two lanes. The PMB is a full-scale laboratory that has over 200 sensors installed and used as needed for each bridge study. 100 strain gauges were installed on the six steel girders on the top and bottom flags of the PMB steel girders. Only 6 strain gauges were used in this research that are located at the bottom flange of steel girders at the mid-span of the center-span, one per girder. The temperature sensors between concrete and steel girders were also utilized to obtained temperature in the proposed method.

Fig. 35. Picture of PMB and DAQ System

The method used in the proposed system does not have the capability of using measured response of the bridge when there are multiple vehicles on the bridge

simultaneously. Only single truck events were used in the proposed method. A single truck event is the traffic event that there is only one vehicle on the bridge during the traffic event. Traffic events that involve multiple vehicles simultaneously are automatically identified and discarded. The details of removing the multiple vehicles events can be found in the paper by Zhao et al. (2016) and Reiff et al. (2016). During one year of continuously recording, the DAQ system obtained 2200 single heavy truck events. The collected single heavy truck events were used to develop the multiple regression models and to build the distribution of detrended GDFs for the healthy bridge.

A prototype system was developed for concept proofing. A Microsoft Azure Virtual Machine (VM) was used as the cloud-computing hub. Microsoft Windows Server 2012 was chosen as the operating system on the VM. The mongoose web server was utilized to host the HTTP communication. The communicating and processing programs were all written in Python. A preliminary website was developed with Django framework in Python. The software packages and platform were chosen based on the consideration of easy deployment and low cost.

4.4 Detrended GDF Methodology for Bridge Condition Assessment

Many methods can be used to detect bridge damages and to assess bridge conditions. The detrended GDF methodology was utilized in this prototype of cloud-based real-time bridge monitoring system because of the method can achieve the real-time recommendations by performing a statistical hypothesis test on detrended measured GDFs. Zhao et al. (2016) showed that the proposed detrended GDF methodology could detect bridge damages with a high likelihood that the damage is detected when the bridge is truly damaged.

A Girder Distribution Factor (GDF) is defined as the percentage of total live load carried by a bridge girder when the girders are identical (Ghosn et al. 1986). The GDF can be calculated from measured strains as

$$GDF = \frac{\varepsilon_i}{\sum_{j=1}^{N} \varepsilon_j} \tag{24}$$

Where ε_i denotes the strain measurements from the ith girder, N is the total number of girders. Damaged bridges experience a change of stiffness that is also reflected in the way in which loads are distributed over the structure (Kim et al., 2008; Comanducci e. al., 2016). GDF is an effective index for bridge damage, but it can be affected by non-structural effects such as bridge age, temperature, frozen ground, and truck travel path. These non-structural effects introduce errors that may change the cumulative distribution function (CDF) of GDFs for a healthy bridge resulting in false alerts. In addition they can introduce errors that may change the cdf of GDFs for a damaged bridge and resulting in not giving an alert when it is necessary.

The damage detection system that is based on hypothesis test can give a false recommendation if the GDFs' distribution is dependent on the non-structural factors. To improve the accuracy of damage detection, the non-structural effects were removed to provide a consistent index for bridge damage detection. A multiple regression model was developed and then used to remove the GDFs variation due to the non-structural effects leading to detrended GDFs that can only be influenced by potential damages.

A statistical hypothesis test framework for bridge damage detection using GDFs was first introduced by Reiff et al. (2016). The Wilcoxon rank-sum test, a nonparametric approach to detect the difference between two sets of samples (Wilcoxon, 1945), was adopted in this framework. In the proposed method, the most recent 50 events, which is

approximately the average number of single heavy truck events collected for a week, were considered as the recent sample set. All the collected events were considered as the base sample set. The Wilcoxon rank-sum test was performed between the recent sample set and the base sample set for the detrended GDFs with a given significant level. The outcome variable from the rank-sum test, *h*, is a binary variable equal to 0 or 1, with a value of unity implying that the recent sample set is different from the base sample set. Reiff et al. (2016) defined a bridge Damage Index (DI) as

$$DI = \frac{\sum_{i=1}^{N} h_i}{N} \tag{25}$$

The DI can be interpolated as the number of girders that has a different distribution of detrended GDFs with the calibrated condition as a fraction of all girders considered.

Follen et al. (2014) introduced a bridge signature which can be used to assess bridge health condition by predicting the possible location of the damage. Bridge signatures are developed with a nonparametric empirical CDF for the detrended GDFs. The bootstrap method, a generalized resampling approach, was used to construct the CDFs of the detrended GDFs. Each bootstrap sample set was chosen randomly with replacement from the base sample set of detrended GDFs. The sample size used in this method was 50 events. The bootstrap resampling procedure was repeated 1000 times, creating 1000 samples of 50 detrended GDFs. In each sample, the 50 detrended GDFs were sorted in ascending order. At each rank, the largest 2.5% and the smallest 2.5% of the 1000 samples are removed to create a 95% tolerance interval, that can also be defined as bridge signature envelope. The recent sample set can be plotted as girder signature with the 95% tolerance interval. In areas that the girder signature is outside the tolerance interval, it indicates some form of structural change or damage. If the girder signature is above the envelope, that girder is picking up an additional load from adjacent possibly damaged girders. If the girder

signature is below the envelope, that girder has lost some capability of carrying loads. Reiff et al. (2016) used a calibrated FEM developed by Sanayei et al. (2012) to simulated the damage and response. Zhao et al. (2016) utilized the simulated responses of the model with various damage types to construct Fig. 36 demonstrating the capability of assessing bridge condition.

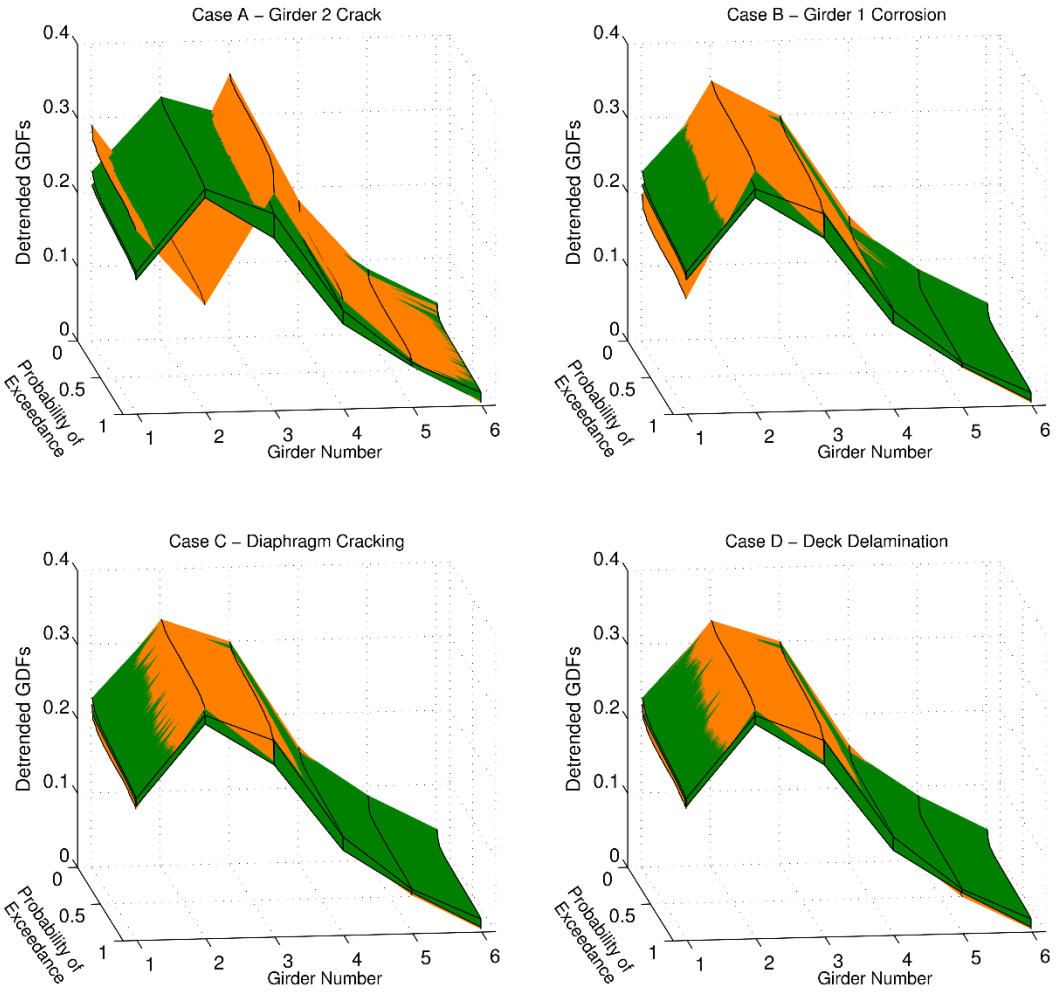

Fig. 36. Bridge Signature Surface of Detrended GDFs

In Fig. 36, envelopes corresponding to the sets of bridge signatures for all girders were combined in a 3D plot to create a bridge signature surface. For each girder, the upper

and lower 95% tolerance value are plotted against each probability of exceedance. The upper and lower surface defined the bridge signature tolerance interval of a healthy bridge. Bridge signature surface for each damage scenario was also plotted in the figure. The proposed method is more powerful to detect damage on girders rather than other structural components because the strain gauges were located on the bottom flange of girders at midspan. In order to have accurate bridge condition assessment, the locations of sensors can be optimized by future studies.

The proposed method will only perform a rank-sum test to detect possible bridge damages and only plot 50 data points to find the possible location of damages during daily recommendation making routine. The required computing time for one bridge is within seconds using a conventional lab computer, which makes it possible for real-time recommendation making.

4.5 Case Study: Prototype of BHP using Detrended Bridge Girder Distribution Factors

There are three parts of the prototype of Bridge Health Portal (BHP): Smart Bridge, Cloud Computing Hub, and Control Center. The BHP interface and the system architecture for bridge instrumentation, DAQ, data communication, and cloud computing for Real-Time Bridge Condition Assessment are shown in Fig. 37. The programming flowchart of the prototype of BHP is shown in Fig. 38.

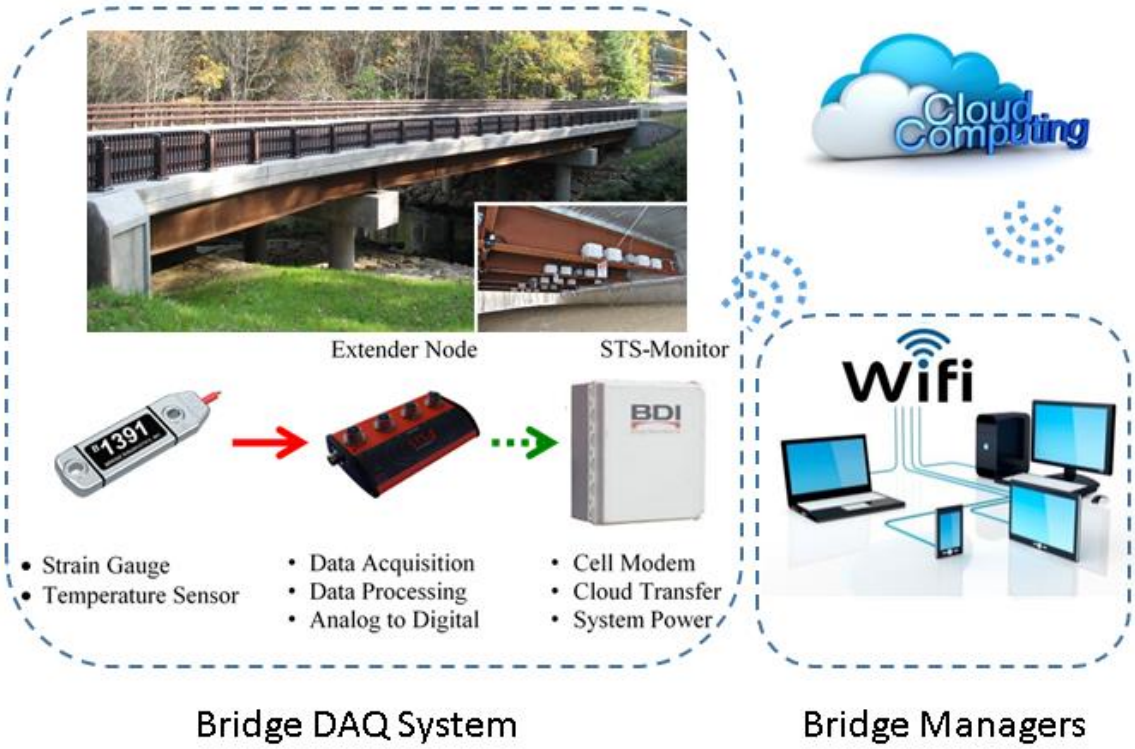

Fig. 37. Architecture for Bridge Health Portal

The DAQ system and on-site computer can collect, process, and transfer the data to the cloud computing hub. In the prototype of BHP, the on-site computer, that receives the data from the DAQ system, performs the preliminary computation to identify events that can be used for structural condition assessment. Only the GDFs and temperature are transferred to the cloud computing hub. Processing data at the smart bridge can reduce the demand for data transfer. A lab computer was used as a smart bridge to simplify demonstration. Collected raw strain measurements were saved on this computer. A program on the lab computer processed the raw strain measurements to identify single heavy vehicle events. The corresponding detrended GDFs and temperature data were transferred to the cloud computing hub for the process.

The cloud computing hub was based on a Microsoft Azure Virtual Machine, where data will be stored, analyzed, and presented. The database has the basic information for

each bridge as well as the collection of detrended GDFs from traffic events. The hypothesis test was automatically performed on the base sample set and a recent sample set when a new traffic event was delivered. The bridge signature was also constructed by the automated program on the cloud computing hub. The structural health conditions are published on a website hosted on the cloud computing hub. If the bridge damage index is above the trigger level, the alerts will be sent by automated emails, text messages, or phone calls according to the level of possible damages.

The predicted bridge conditions are published on a private website for security purposes. The bridge owners and manager can access their designated sites conveniently by using a user ID and password. An interactive website helps the bridge owners and managers to make a decision by visualizing the bridge conditions and recommendations. A list view was designed to show the conditions of different bridges, which allows the bridge engineers to monitor many bridges on one screen. Another detailed view was developed to show the detailed information and bridge signatures for a specific bridge, which can be used for comprehensive monitoring. The website allows different levels of user administration, which allows the bridge owners and engineers to collaborate their bridge evaluations and inspections.

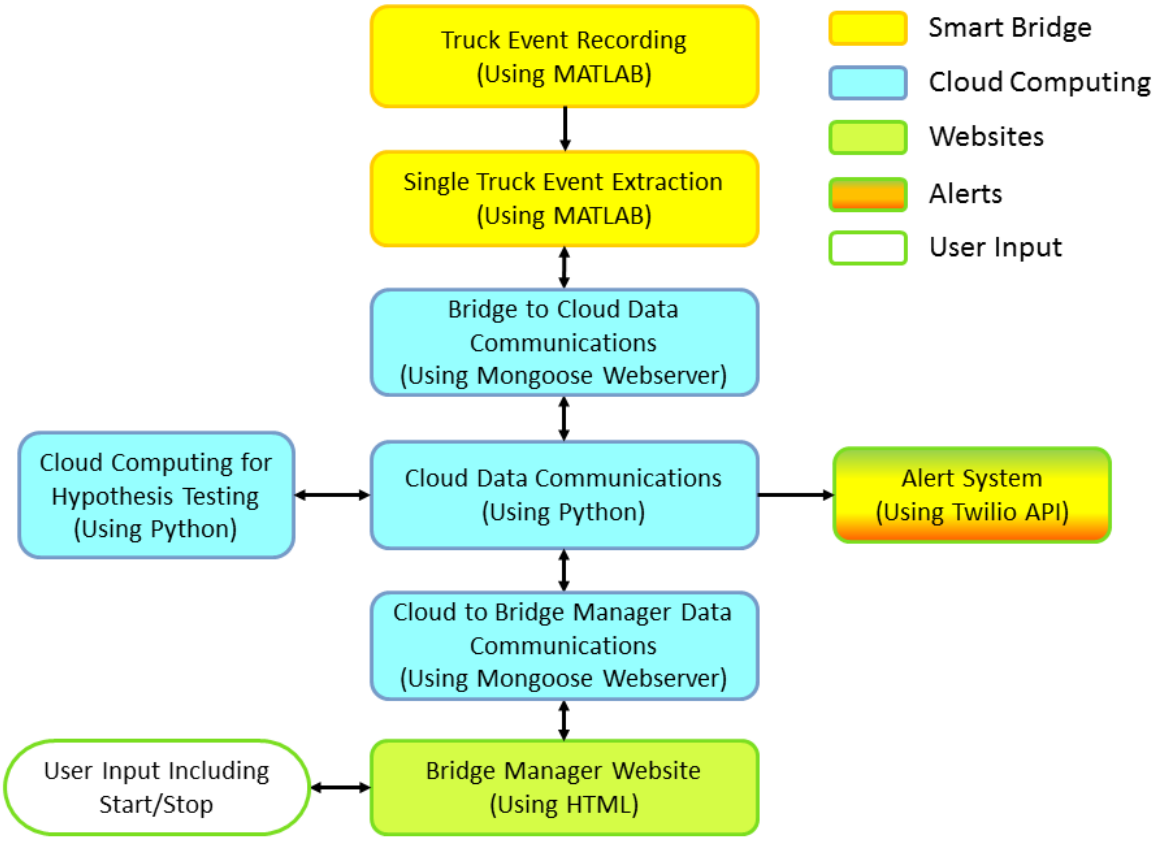

Fig. 38. Bridge Health Portal Architecture Flowchart

4.6 Discussion of Liabilities

It is recommended that the Bridge Health Monitoring consultants install, calibrate, and maintain the bridge monitoring equipment and software to ensure that the outcome from the BHP is tailored to their needs and is reliable. However, the damage trigger levels shall be determined by the bridge owner/manager. These trigger thresholds can be easily changed as the bridge managers gain experience with the software. In addition, the damage trigger levels can be set by minimizing the overall costs as recommended by Field et al. (2004) for minimizing the cost of environmental management decisions by optimizing the statistical thresholds.

Instead of making decisions about bridge posting, closure, and repair, the BHP shall be monitoring the response and only make recommendations based on changes in bridge's response to traffic events. When the BHP detects changes above the recommended thresholds in the distribution of GDFs, it can only tell the bridge manager that the live load distribution of the bridge has changed and there is a high probability that the stiffness of one or more bridge components has changed. The bridge manager can also observe the areas that have shown significant changes based on reports similar to Fig 2. The recommendation shall be a specific, measurable, and objective describing the relative magnitude and location of the bridge damage. The proposed BHP can be considered as an on-site inspector looking at the bridge 24/7 and making observations of potential changes. The virtual inspector can also transfer its observations to the bridge managers for decision making in real time.

The Bridge owner or manager should decide in which situation the bridge shall be closed for the sake of safety issue. It is the structure's owner/manager's responsibility to make the inspection decision to check the structure's health condition, if the BHP sends an alert. Besides the proposed system, the structures shall be inspected or evaluated according to the established guidelines and regulations. The bridges in the US are required to be inspected for every 24 months. The inspection is mainly based on the visual inspection. Normally, there is no inspection until the next scheduled 2-year inspection unless there is a specific concern. The proposed BHP can fill the gap between inspections, and also can detect early changes and potential damages that may be missed by visual inspections. The BHP was developed to accommodate the Federal Highway Administration (FHWA) and State bridge inspection regulations. Besides, The BHP can be adjusted or expanded based on requests of Department of Transportations (DOTs). Installing the proposed BHP can be considered as a more objective supplement for government regulations.

4.7 Conclusions

The proposed system provides a measurement-based and objective evaluation of the bridge performance with 24/7 monitoring capability and alert system. To prove the concept, a prototype of the system was developed using Microsoft Azure Virtual Machine (VM) and two lab computers. One of the computers acts as a fully instrumented bridge that can record the strain response of heavy vehicle traffic events, preliminarily process the recordings, and transfer the traffic events to the cloud-computing hub. The VM is acting as a cloud-computing hub where traffic events are processed and stored for bridge condition assessment. The bridge performance recommendations are published on a secure website that is also hosted on the VM. Another computer can act as the Bridge Health Portal that grants the access for bridge engineers or the bridge managers/owners from any remote location. The proposed system for bridge condition assessment adopted hypothesis testing framework and bridge signature using detrended GDFs. The paper also discussed the capability, limitation, responsibility, and liability related to the real-time continuous bridge monitoring for condition assessment.

4.8 Future Works

Both hardware and software can be improved for the proposed system using newer transducers, data acquisition systems, communication systems, and faster computers. Installing the wireless sensors can solve the wiring problems for existing bridges, which improves the feasibility of applying the proposed system to existing bridges. Low noise sensors can improve the signal to noise ratio. More powerful on-site computing module can reduce the time for single heavy vehicle event identification and processing. Many other hardware improvements can be made per the requirements of DOTs. The software can be improved by utilizing more bridge damage indicators, by adopting more sophisticated algorithms, and by using more efficient programs. The data security issues

beyond using user IDs and passwords can be addressed in the future improvements. The bridge owners need to protect their equipment and data from being stolen or destroyed. All data transferred between smart bridge and cloud computing hub shall be encrypted by Secure Sockets Layer (SSL). For future versions of the system, the performance can be improved, the service stability can be increased, and the cost can be further reduced.

The BHP can also be enhanced by adding new features, such as capturing images, automatic identification of license plate, and traffic volume monitoring and analysis. Not only can be used for bridge condition assessment, BHP can also be used for law enforcement and traffic controls.

Economic studies about the cost of applying the proposed Bridge Health Portal and the savings for early damage detection for bridges can be performed. The cost of SHM is only a fraction of the cost of bridge. Early detection of damages not only can reduce the cost of rehabilitation but can also increase bridge safety and prevent possible disasters. More sophisticated economic analysis can reveal that obtaining additional information about bridge health condition reduces the life cycle cost for bridges.

4.9 References

Al-Radaideh, A., Al-Ali, A. R., Bheiry, S., & Alawnah, S. (2015). A wireless sensor network monitoring system for highway bridges. In *Electrical and Information Technologies (ICEIT), 2015 International Conference on* (pp. 119-124). IEEE.

Comanducci, G., Magalhães, F., Ubertini, F., & Cunha, Á. (2016). On vibration-based damage detection by multivariate statistical techniques: Application to a long-span arch bridge. *Structural Health Monitoring*, 1475921716650630.

Doebling, S. W., Farrar, C. R., Prime, M. B., & Shevitz, D. W. (1996). Damage identification and health monitoring of structural and mechanical systems from changes in their vibration characteristics: a literature review (No. LA--13070-MS). Los Alamos National Lab., NM (United States).

Farrar, C. R., & Worden, K. (2012). Structural health monitoring: a machine learning perspective. John Wiley & Sons.

Field, S. A., Tyre, A. J., Jonzen, N., Rhodes, J. R., & Possingham, H. P. (2004). Minimizing the cost of environmental management decisions by optimizing statistical thresholds. *Ecology Letters*, *7*(8), 669-675.

Follen, C. W., Sanayei, M., Brenner, B. R., & Vogel, R. M. (2014). Statistical bridge signatures. *Journal of Bridge Engineering*, *19*(7), 04014022.

Ghosn, M., Moses, F., & Gobieski, J. (1986). Evaluation of steel bridges using in-service testing. *Transportation Research Record*, (1072).

Kim, Y. J., Green, M. F., & Wight, R. G. (2008). Live load distributions on an impact-damaged prestressed concrete girder bridge repaired using prestressed CFRP sheets. *Journal of Bridge Engineering*, *13*(2), 202-210.

Li, H. N., Ren, L., Jia, Z. G., Yi, T. H., & Li, D. S. (2016). State-of-the-art in structural health monitoring of large and complex civil infrastructures. *Journal of Civil Structural Health Monitoring*, *6*(1), 3-16.

Malekzadeh, M., Atia, G., & Catbas, F. N. (2015). Performance-based structural health monitoring through an innovative hybrid data interpretation framework. *Journal of Civil Structural Health Monitoring*, *5*(3), 287-305.

Sanayei, M., Phelps, J. E., Sipple, J. D., Bell, E. S., & Brenner, B. R. (2012). Instrumentation, nondestructive testing, and finite-element model updating for bridge evaluation using strain measurements. *Journal of bridge engineering*, *17*(1), 130-138.

Sartor, R. R., Culmo, M. P., & DeWolf, J. T. (1999). Short-term strain monitoring of bridge structures. *Journal of Bridge Engineering*, *4*(3), 157-164.

Reiff, A. J., Sanayei, M., & Vogel, R. M. (2016). Statistical bridge damage detection using girder distribution factors. *Engineering Structures*, *109*, 139-151.

Wilcoxon, Frank. (1945). "Individual Comparisons by Ranking Methods." Biometrics Bulletin 1 (6): 80-83.

Yang, M. (2015). An Integrated Real-Time Health Monitoring and Impact/Collision Detection System for Bridges in Cold Remote Regions (No. MPC 15-282).

Appendix A Additional Figures for Detrended GDFs method

This Appendix contains the materials could not be included in Chapter 3 due to space limitation. Fig. 39 to Fig. 43 are the quantile plot of GDF for the rest of girders. Girders under southbound traffic lane have larger variation compared to girders under northbound traffic land and sidewalk. The reason is there are more heavy truck event in southbound. Fig. 44 to Fig. 48 demonstrate the quantile plot of GDF residuals for the rest of girders. The most variation of GDF has been removed in the residuals, which improves accuracy of damage detection based on hypothesis test framework. 7

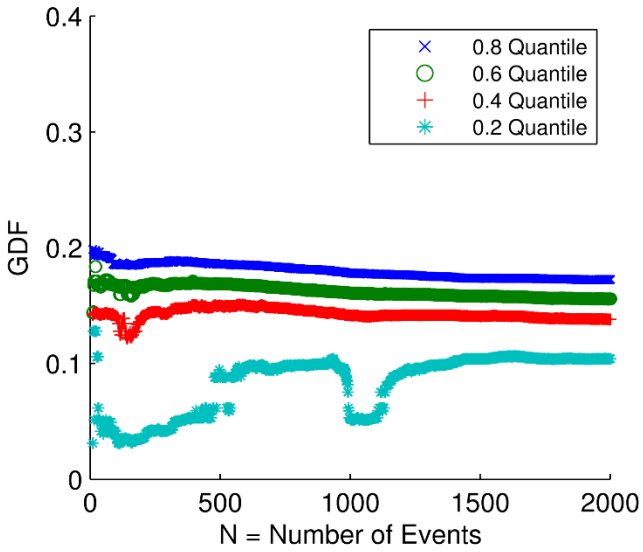

Fig. 39. Quantile Plot of GDF for Girder 1

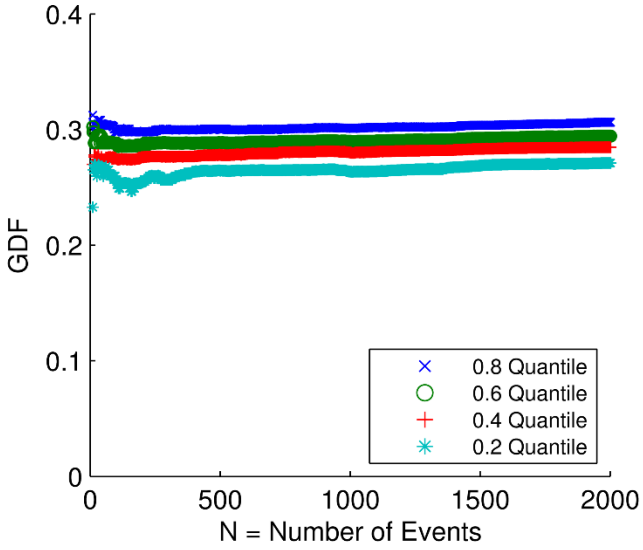

Fig. 40. Quantile Plot of GDF for Girder 3

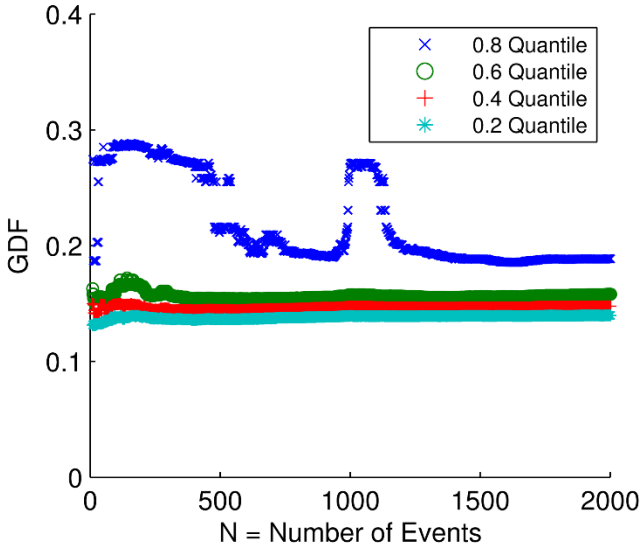

Fig. 41. Quantile Plot of GDF for Girder 4

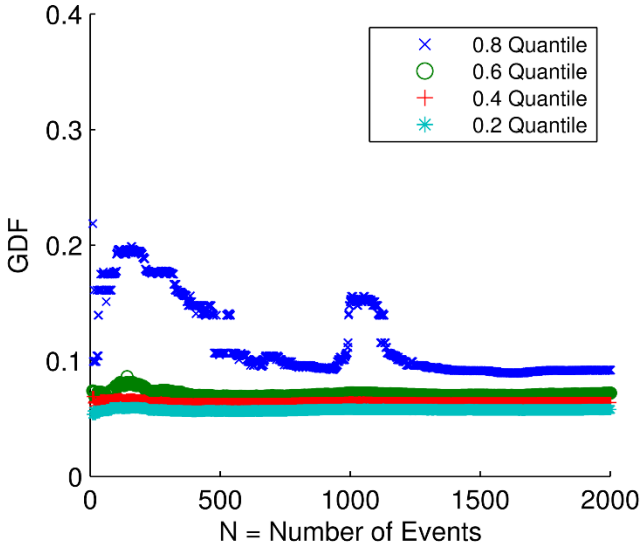

Fig. 42. Quantile Plot of GDF for Girder 5

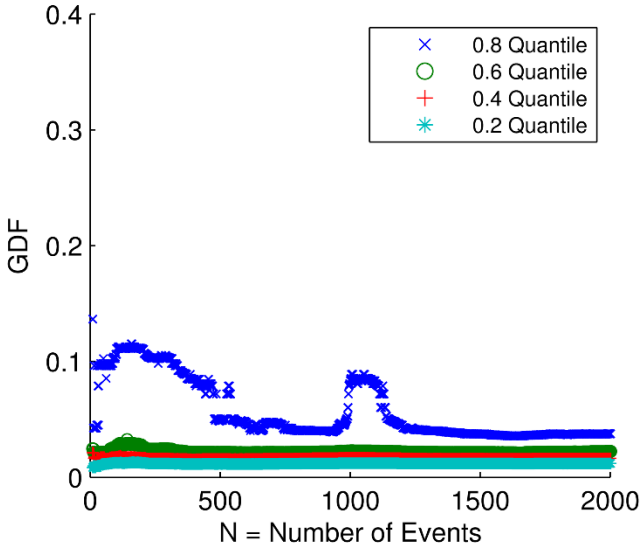

Fig. 43. Quantile Plot of GDF for Girder 6

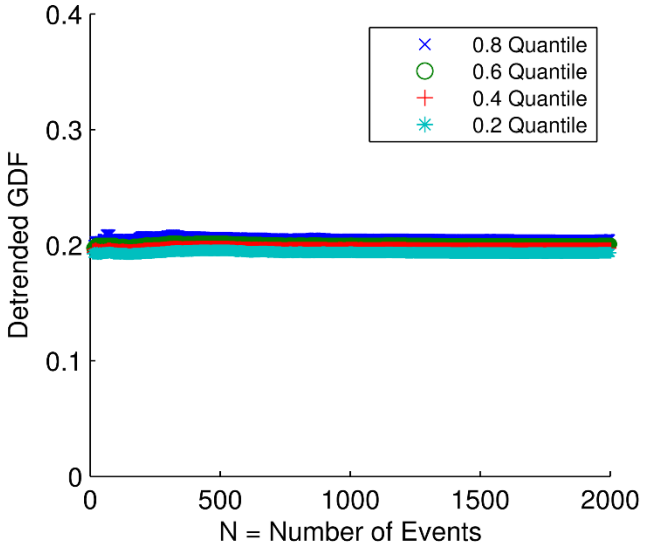

Fig. 44. Quantile Plot of GDF Residuals for Girder 1

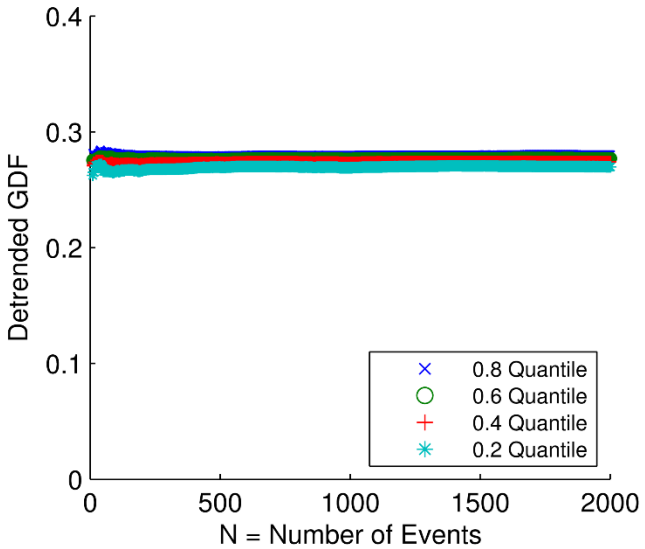

Fig. 45. Quantile Plot of GDF Residuals for Girder 3

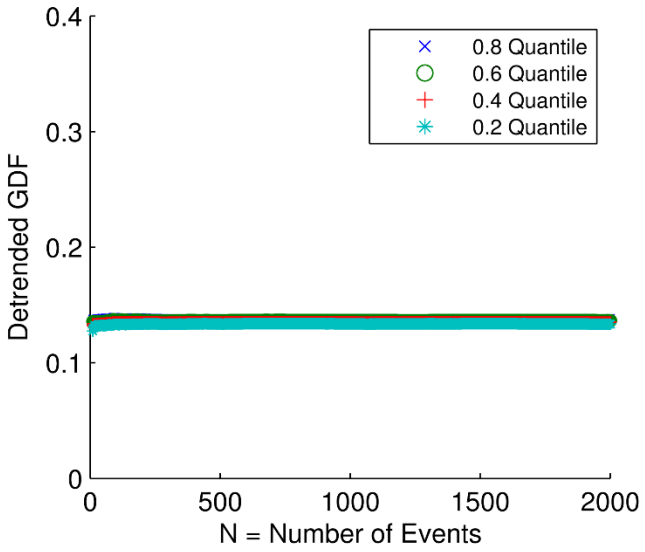

Fig. 46. Quantile Plot of GDF Residuals for Girder 4

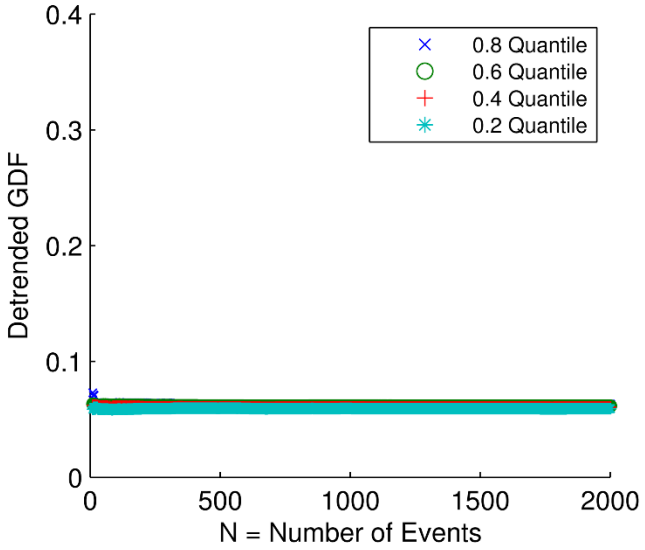

Fig. 47. Quantile Plot of GDF Residuals for Girder 5

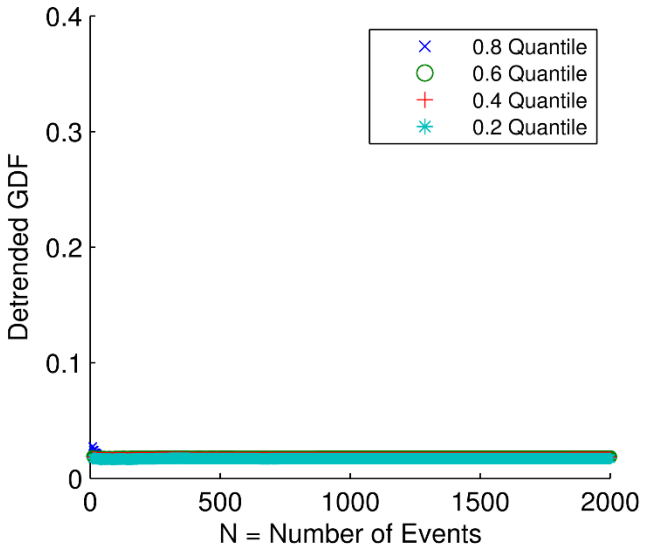

Fig. 48. Quantile Plot of GDF Residuals for Girder 6

Fig. 49 shows the normal probability plot of GDF residuals for each girder. The model residuals associated with the models for girders 1 and 2 exhibit approximately normal behavior, but other girders do not exhibit normality in the tails of the distribution of residuals. This is likely due to the fact that there are other environmental factors or traffic event factors that are not included in the regression model and the model itself is only an approximation of reality so that its structure could be improved. The violation of OLS assumptions indicates there is still room for improvement and we must be careful when interpreting the resulting p values in Table 2, since their interpretation is only reasonable when the model residuals are well behaved in the sense described above.

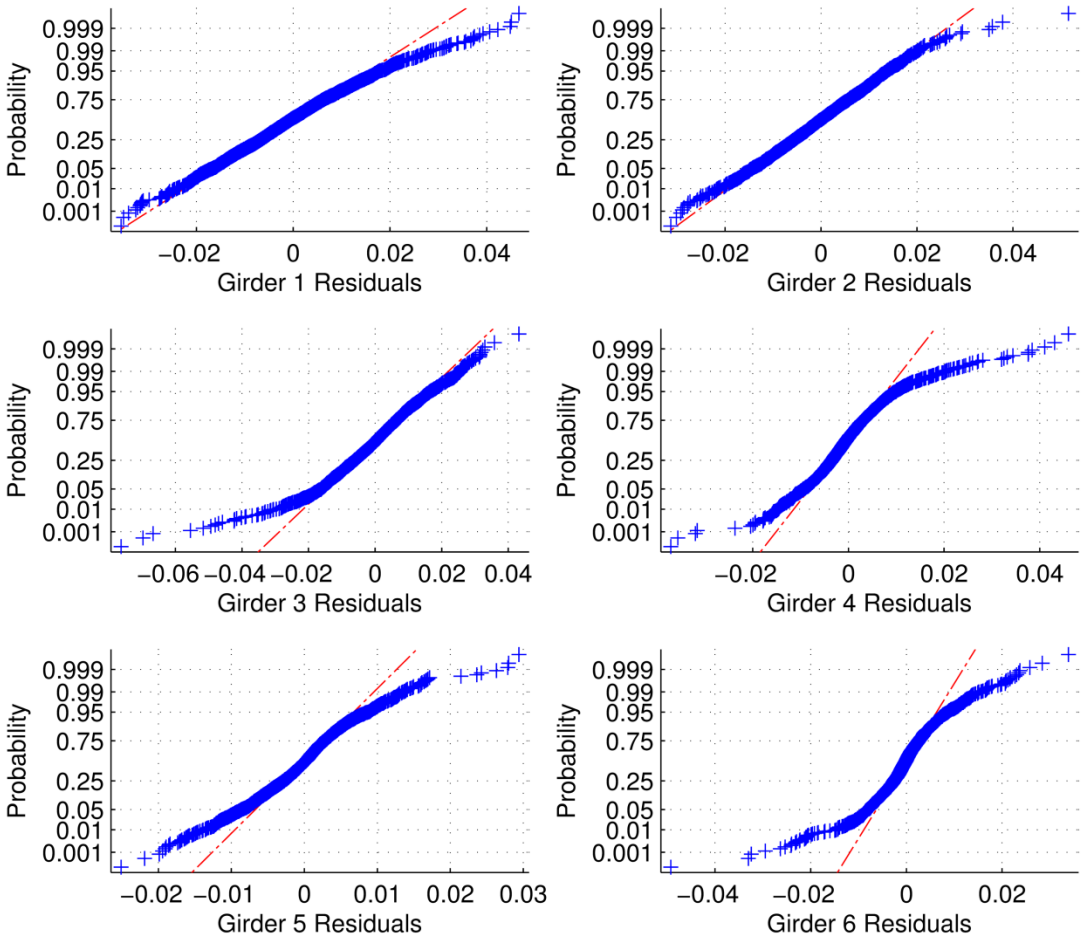

Fig. 49. Normal Probability Plot for GDF Residuals

Fig. 50 to Fig. 55 show the comparison between measured GDFs calculated from measured strain response and predicted GDFs calculated from fitted multiple regression model. The plots show that the measured GDFs agree with the predicted GDFs, which indicates that the fitted multiple regression model of GDFs can mimic the measured GDFs.

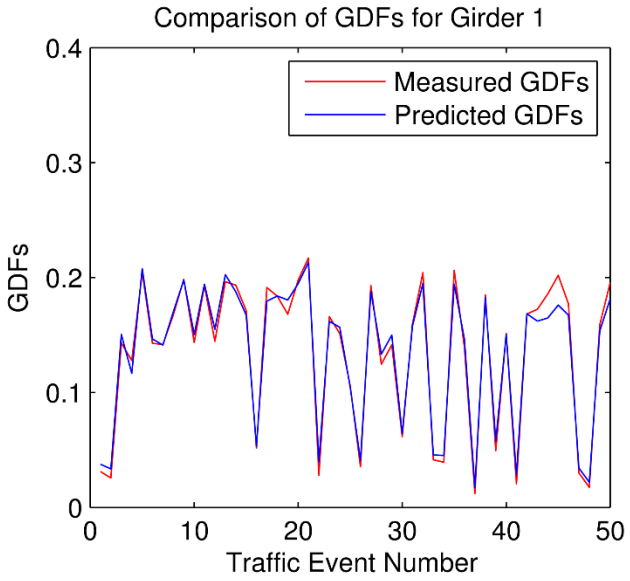

Fig. 50. Quantile Plot of GDF Residuals for Girder 1

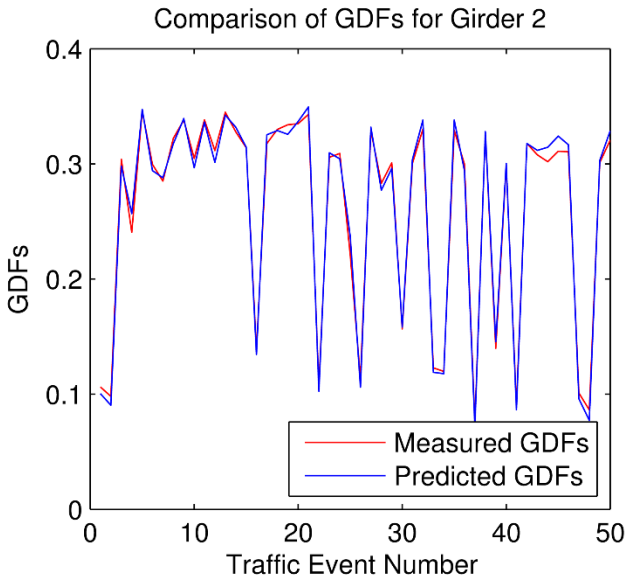

Fig. 51. Quantile Plot of GDF Residuals for Girder 2

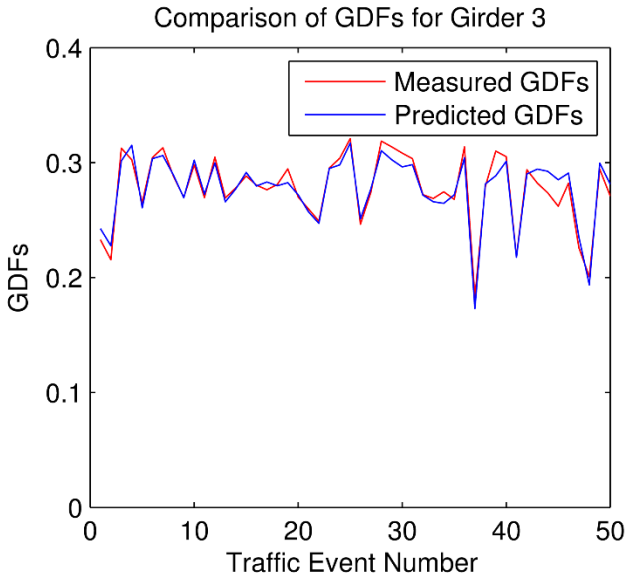

Fig. 52. Quantile Plot of GDF Residuals for Girder 3

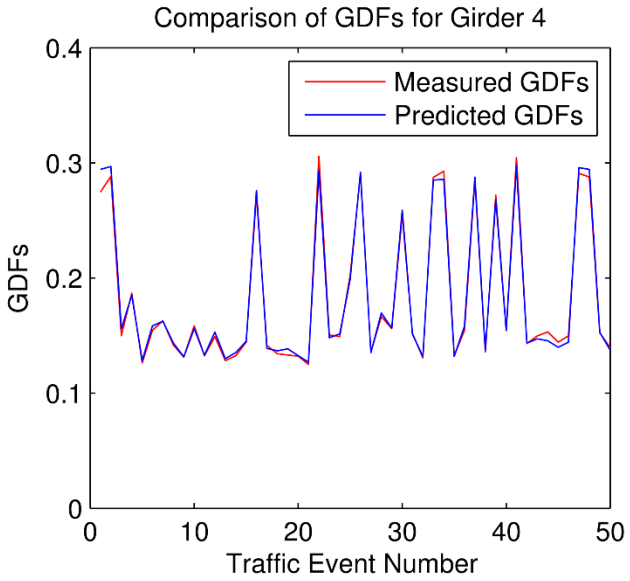

Fig. 53. Quantile Plot of GDF Residuals for Girder 4

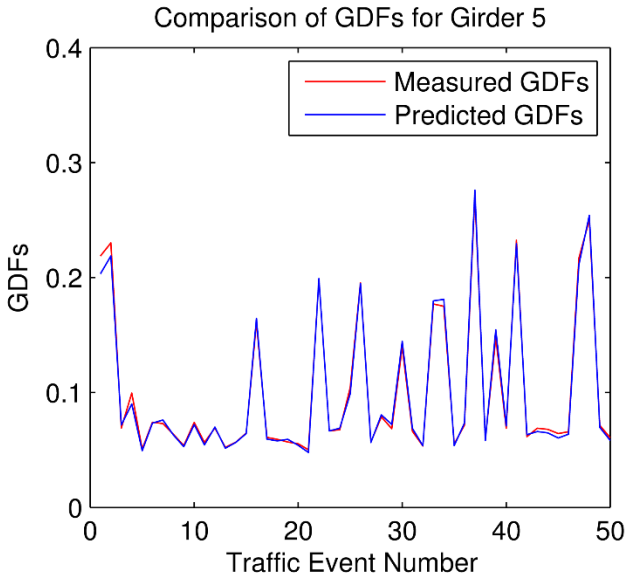

Fig. 54. Quantile Plot of GDF Residuals for Girder 5

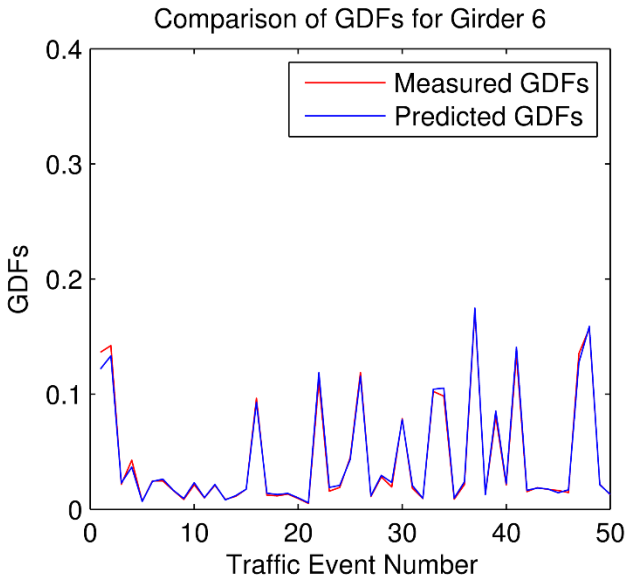

Fig. 55. Quantile Plot of GDF Residuals for Girder 6

Fig. 56 is the minimum damage detection level with significance level equals to 5%. For each GDF increment, the corresponding Type II error are plotted. The blue line is the 5% type II error line. From the intersection of blue line and the black line, the minimum damage detection level for 5% significance level and 5% Type II error can be obtained.

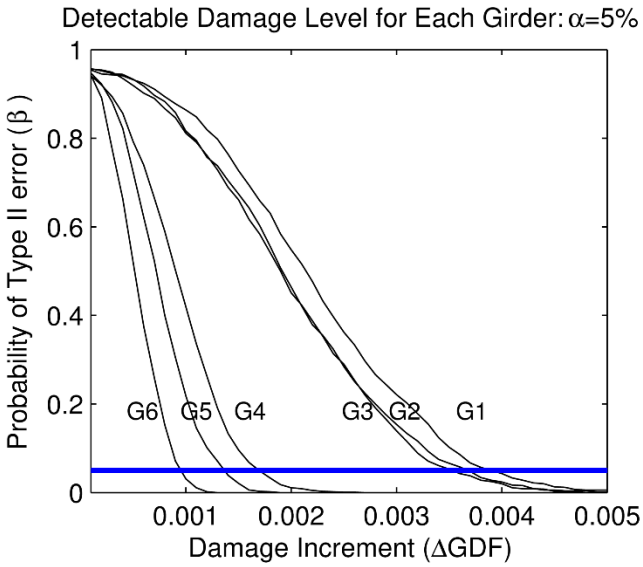

Fig. 56. Minimum Damage Detection Level